uc3m | Universidad Carlos III de Madrid

University Degree in Biomedical Engineering

Academic Year 2018-2019

Bachelor Thesis

"Characterization of printable electrical sensors applied to cellular cultures"

Rosario Quevedo de Cea

Pablo Acedo Gallardo

Universidad Carlos III, Madrid, June 2018-June 2019

ABSTRACT

Impedance biosensors have turned in a special interest as label-free and low cost platforms for real time detection of biological phenomena. The objective of this study was to characterize a given model of an interdigitated electrode sensor (model 1) manufactured by inkjet printing technology over a flexible substrate (PET). This characterization was applied to HaCaT cellular cultures at different confluences in order to distinguish an impedance response first associated with the cellular presence and then proportional to the cellular confluence of such presence.

With this aim in mind, impedance spectroscopy principle was employed as the main analysis method. From the empirical impedance response, electrical equivalent circuits were obtained by fitting the empirical values with theoretical circuit's elements. In addition, inverted and scanning electron microscopes were used in order to visualize the whole process, as a way of ensuring that the electrical changes recorded had a real and relevant biological meaning.

Three different conditions were tested over the sensor: culture medium without cells, HaCaT epithelial cells seeded over the sensor at 40% of confluence and at 80% of confluence. Impedance responses were recorded each 2 h during 36 h.

Results obtained showed that at some point the cellular presence changed the equivalent electrical circuit when compared with the control measurements performed without cells. This change in the circuit has been associated with the cellular attachment of the cells on the IDE, which, as it was later confirmed by the visualization of the cellular culture, has been identified to take place from 22 h on and coincides with the presence of an additional time constant in the electrical circuit. Moreover, the constant phase element of such equivalent circuits was compared for the three conditions, obtaining that its variation is inversely proportional to the area covered by the cells on the sensor. The main drawback encountered during the process was the noise coming at low frequencies that compromise the measurement from 0,1 Hz to 10 Hz.

In conclusion, this work has been useful to prove that IDEs can provide an impedance response associated to cellular presence. Based on the main findings, another setup to reduce the noise was proposed (solution design: model 2) and tested for the following experiments, reporting good results.

Key words: impedance biosensors, IDE, impedance spectroscopy, cellular culture.

INDEX OF CONTENT

INDEX OF FIGURES

INDEX OF TABLES

1. Introduction

1.1 Motivation and goals

Over the last decades, there has been an increased interest in combining the field of Electronics with Biology. This emerging field, called Bioelectronics, seeks to integrate the microelectronics principles with the biomolecular laws. The consequences that this new approach has are being of special interest in the medical research field, with a wide variety of different applications such as fuel cells, biomimetic systems, bionics, brain interfaces, Lab-on-a-chip and biosensors, which were the objective of this Bachelor Thesis.

Biosensors are defined as analytical devices incorporating a biological material, a biologically derived material or a biomimic [1]. The basic interface of a biosensor consists of three phases: the detection of the biological phenomenon, the amplification of the resulting signal and finally its conversion to the digital domain.

Electrical biosensors are nowadays one of the bigger promises in Bioelectronics, because of their low cost, low power and their ease of miniaturization. Besides these advantages, they provide the user with a real-time measurement, which makes electrical biosensors a suitable device for covering point-of-care diagnostics as well as detecting biowarfare agents. [2]. Electrical biosensors can be classified into three different groups, according how the electrical measurement is made: voltammetric and amperometric biosensors, which employ DC voltage to measure changes in the potential (voltammetric) or in current (amperometric) under different medium conditions, and impedance biosensors, which measure the electrical impedance of an interface under AC steady conditions [2]. This last measurement is normally repeated for different frequencies, in order to identify the most sensitive frequency range. The voltage-to-current ratio gives the impedance, and this approach, as it will be further discussed (see point 2, State of the art, and specifically 2.1) is known as Electrochemical Impedance Spectroscopy (EIS). It must be remarked that impedance measurements are performed without the necessity of adding special reagents and can operate in label-free mode, which reduces the overall cost of the device.

The use of interdigitated electrode sensors (IDE) is widespread as a suitable platform to apply a given current and record the cellular culture response. IDEs have evolved from the single two-electrode configuration until its actual miniaturization in an electrode array assembly, which guarantees a better sensitivity and operability (see 2.3 for further information). At the present time, electrochemical impedance spectroscopy is being used to characterize many biological phenomena such as the electrical detection and characterization of bacterial adhesion [3], the detection of biomolecules by label free methods [4] or even the characterization of the biological media [5].

In this Bachelor Thesis, interdigitated electrode biosensors were employed to associate changes in the impedance with relevant cellular phenomena such as cell pre-attachment and cell attachment. For this purpose, the electrical measurement was performed using an impedance/phase analyzer device and a picoamperimeter. The change of the field generated will be registered in terms of electrical impedance, in the case of AC voltage (impedance/phase analyzer), and conductivity (picoamperimeter), when dealing with DC voltage.

The aim of this multiple characterization was, in the first place, to use the first sensor (model 1) to fully understand the impedance spectroscopy principles when applied to a biological cellular culture: identifying the equivalent circuit elements providing relevant information as well as the critical frequencies where the device is more sensitive. Once this goal was achieved, the next step was to make a solution design proposal with other two models (model 2 and model 3) by altering parameters such as the spacing of the electrodes or the electronic ink used to print sensors to try to solve some of the issues encountered along the path.

All the essays were made in an *in vitro* 2D cellular culture, under a controlled environment. However, as modern medical challenges start by the necessity of the real-time detection of multiple human physiological parameters, this work has always bore in mind the future implantation of the interdigitated sensor in a patient, making the pertinent readjustments of the sensor design for a suitable *in vivo* implantation. There is still a long way to go, but all the paths start with a few steps.

1.2 Socio-economic impact. Medical scenario: severe burns and sepsis

Thermal injury depends on both the time of exposure and the exposure temperature, but there is still a common denominator in burn injuries: protein denaturation and cell death either by apoptosis or by necrosis [6]. Severe thermal injury patients suffer from profound morbidity and mortality [7].

Since one of the main challenges in treating acute thermal injuries is preventing infection, excising the eschar and covering the wound are critical and must be done as fast as possible [9]. The current treatment for thermal injury relies on the coverage of the wound to restore the skin function after damage. In the cases of localized and reduced burns, autograft or skin graft, coming from an uninjured donor site on the same patient, is the first and best option [9]. However, due to the extension of the burn injury, there are cases in which autografts are not an option. These cases are the scope of this work.

Patients with more extensive burns require a rapid temporary coverage of their wounds in order to prevent burn wound colonization by bacteria [9]. There are three main possible commercially available coverages. Allografts, commercialized nowadays as Alloderm or GraftJacket, which consist of acellularized matrices coming from humans [9]. Xenorafts, which are acellularized matrices coming from other species such as bovine or shark matrices, commercialized by companies such as Integra. The last commercially available strategy goes a step further and consists of creating a graft made of patient's own skin. These cultured epithelial autografts are nowadays commercialized as Epicel [10]. Epicel provides a permanent skin replacement made of patient's own human keratinocytes (epidermal layer of the skin).

The problem with these approaches is that epidermal substitutes are normally only a few cellular layers thick and lack normal dermal components [9]. Even Epicel, which is nowadays the only treatment employing patient's own cells cultured grafts approved by the FDA [10], lacks the rest of the components on the skin, replacing just the most superficial part of it. The challenge now is to construct dermo-epidermal equivalents including both the dermal and the epidermal layers of the skin aiming to reconstruct a functional human skin to replace the lost of this tissue.

Nowadays, burn care has achieved unprecedented survival rates; nevertheless, there are still some medical challenges to fight with when dealing with severe burn patients. The most common complications these patients are exposed to consist of bacterial infections, followed by pneumonia [8]. In the case of bacterial infections, the rates of sepsis-related death are 50%–84% in adult burn patients and ~55% in pediatric burn patients [7], which is an unmistakable sign of the necessity of an early detection of bacteria presence at the local systemic level, avoiding their proliferation through the human organism that can lead to the patient's death.

The management of burn wound infections has been extensively studied and discussed over the last decades. Although the use of topical antibiotics has reduced the infections considerably, sepsis still occurs [8]. Regarding the actual prevention treatments, recent studies have shown that the employment of quantitative microbiology in burns is limited by the unreliability of a single surface biopsy or swaps sample to represent the whole burn wound [11]. Between both, quantitative tissue biopsies gave a better prediction of sepsis than surface swabs, yet the amount of labor involved in collection and analysis of multiple biopsy samples limit the clinical relevance of this approach [11].

Nowadays, the best approach for the identification of organisms in the septic burn patients includes simultaneous culture of quantitative tissue biopsy, blood, and urine samples [11]. The problem, once again, is the time and amount of labor that these simultaneous analyses take.

In this context, impedance biosensors have turned in a special interest, as they can provide a real time feedback about the changes in the skin surface they would cover. Recent studies have employed impedance sensors to monitor bacteria wounds in dressings [12]. In this kind of approaches, the sensor is placed at the wound-dressing interface and it is designed to measure the conductance changes in the wound's exudate, associating these changes to the presence of bacteria in suspension [12].

In this Bachelor Thesis, we take the first steps in a different approach based on impedance biosensors for the wound monitoring. Instead of aiming to develop a superficial sensor, the following work has been focused on the development of an implantable sensor at the dermis level. An impedance sensor-based device would then play a key role in the early detection of impedance changes at the dermis level in the

presence of bacteria, as well as reporting the information regarding the healing process of the affected dermis.

In other words, our sensor is aimed to provide more information than superficial sensors or superficial biopsies, as it will be placed at the intraepidermal level, and at the same time, it is expected to replace the time consuming of simultaneous biopsies, which in practical terms have a very limited clinical relevance.

2. State of the art

2.1 Electrical impedance measurements background in both cellular culture and tissue

First studies employing cell-covered gold electrodes were reported by Giaever and Keese in 1984; their work was focused on the examination of the dynamical properties of cells in an *in vitro* environment [13].

The principle behind these experiments is named Electrical Impedance Spectroscopy (EIS). EIS is a wide technique used for characterizing in real-time electrochemical systems. The goal of Drs. Giaever and Keese was to apply this principle to cell culture, achieving an in real time biosensing device capable of monitoring cellular changes [13].

In the very first approaches, two gold electrodes were used for measuring bioimpedance, both separated by a confluent cell monolayer immersed in electrolytic medium. They used epithelial cells grown on permeable filters and associated the impedance measurements to cell proliferation, attachment and morphology [13, 14]. Further investigation performed has ended up with multiple electrode configurations and the miniaturization of the multiple sensing electrodes, including the interdigitated electrode sensor (IDE) employed in this work.

Apart from all the mentioned applications involving cellular characterization, EIS principle has been recently evolved through the application in tissue characterization; it has been proved that there is a relation between oxidative stress species and impedance measures in White Rabbits aortas as well as in explants of human aortas, linking the vascular inflammatory responses measured to pre-atherosclerotic lesions [15]. Moreover, EIS is being used for electrical tissue characterization in muscular tissue under different conditions [16].

The reason why this technology has been of particular interest as an *in vitro* assessment relies on the fact that it constitutes a label-free detection method, that is, it does not require special chemical treatments to measure cellular endpoints which can affect the cell behavior [17]. Moreover, its non-ionizing and non-invasive action

principle makes it perfectly suitable to oncology applications, such as tumor cells detection and characterization [18]. Presence of pathogens in cellular culture environment has been also analyzed in terms of impedance changes, proving once again the future perspectives this technique has [17].

2.2 Electrical model on cells and tissue in culture media. Dielectrical properties.

- Electrical model in cells

In order to understand the electronic principles by which cells react to an input current different equivalent circuits have been proposed by the scientific community.

It must be taken into account when working with equivalent electrical models that there is not a single and perfect circuit describing the cells behavior in all the situations; equivalent circuits will vary depending on how well the empirical data matches with the theoretical elements of a proposed electrical circuit. In other words, the equivalent circuit is a theoretical way of processing biological data using electronic elements that will be strongly dependent on the cellular phenomena and the sensor characteristics.

There are two operating modalities using IDEs: faradaic or non-faradaic detection. The difference between both relies on the fact that whereas in faradaic detection the current flows as a result of electronic transfer, in non-faradaic detection the current flows as a result of capacitive nature of an electrode, known as the double layer capacitance [19].

In 2017, in a review of the IDEs' principles [19], the following circuit was proposed when explaining the effect of faradaic detection of cellular phenomena based in the EIS principle:

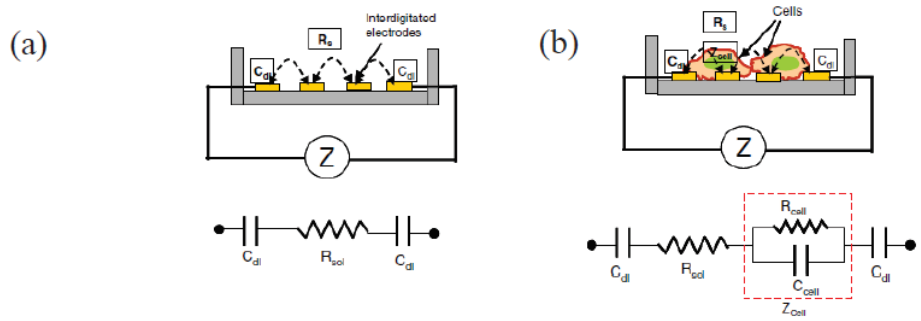

Figure 1 Example of equivalent circuit when dealing with faradic impedance spectroscopy [19]. In a) it can be appreciated that in the absence of cells, the IDE's equivalent electrical circuit is understood as two capacitors in series with a resistor coming from the solution conductivity. In b), the cellular presence produces a change in the equivalent circuit with the addition of another time constant element, that is, the addition of a resistance in parallel with a capacitor.

According to figure 1, the circuit that describes the behavior of the system in the absence of cells includes the capacitances from the double layer of electrodes and the solution parasitic resistance. When cells are added to the solution and become attached to the electrodes, the equivalent circuit includes their impedance contribution as a resistance in parallel with a capacitance. This cell presence results in an overall increment of the total impedance [19].

Different circuits are being used when dealing with faradaic and non-faradaic detection methods. In the following work, non-faradaic detection will be employed for the equivalent circuit fitting and its interpretation (see 4.4.3 for more information regarding the employed equivalent electrical circuits).

➢ Electrical model in culture media

In 2016, it was first described the schematic representation of the equivalent circuit model of an IDE sensor covered with biological medium [5]. This work was based on the well-known fact that when a metal electrode is immersed into a biological medium, a double layer will be formed at the contact interface between the biological medium and the electrode.

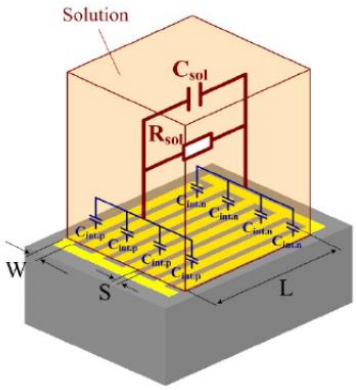

Figure 2. Schematic of the equivalent circuit model of an IDE embedded in biological medium [5]. In this electrical equivalent circuit, C_{sol} and R_{sol} describe the dielectric properties of the medium. C_{sol} stands for the capacitance of the solution and R_{sol} describes the conductive properties of the solution. C_{int-p} and C_{int-n} describe the properties of the double layer [5].

C_{sol} and R_{sol} describe the dielectric properties of the medium. The capacity of the solution is represented by the capacitance C_{sol}; and the resistance R_{sol} describes the conductive properties of the solution. C_{int-p} and C_{int-n} represent the capacitance at the contact surface of each electrode (positive/negative) with the culture medium, representing this way the properties of the double layer. [5] This work characterized the biological media based on conductance changes detected by the impedance sensor.

2.3 Electrical characterization of cells and tissue. Miniaturization, different configurations and main applications of impedance biosensors

In 1991, Drs. Giaever and Keese founded Applied BioPhysics, Inc. to develop, commercialize and market ECIS™ or Electric Cell-substrate Impedance Sensing, which is based in all their previous studies in the electric impedance spectroscopy field [20]. The evolution of their products serve as the perfect example of how the EIS technology has evolved when dealing with cellular culture measurements.

EICS' first design consisted of gold electrode arrays and has evolved to multiple electrode configurations. By reducing the total electrode surface area, the AC current needed for generating the desired electric field also decreases [20]; moreover, reduction in the electrode area allows detecting micro-scale morphological changes of small

population of cells (<100). On the other hand, larger electrodes or multiple electrodes (that is, large collection of small electrodes) measure the average morphological response of many cells (1000+) and this increase in the sample size result in less variability [20]. Besides that, taking advantage of the interdigitated electrode structure allows to increase the effective electrode length thus increasing the overall capacitance.

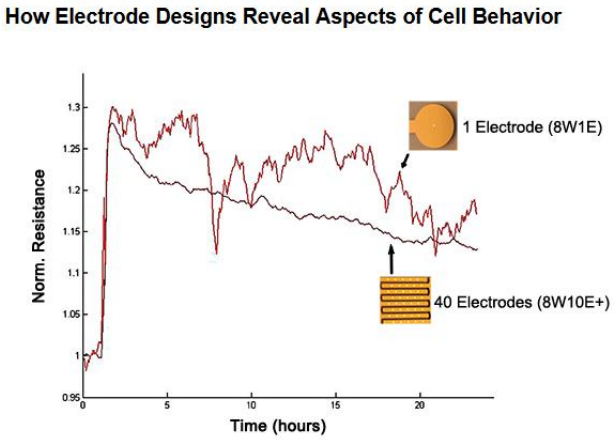

Figure 3. Comparative response between 1 electrode and 40 electrodes configurations of confluent cell layers to the addition of fresh medium [16]. It can be appreciated how the noise is reduced significantly when the electrode array is employed. In addition, the electrode array presents a higher sensitivity in its measurement.

In 2015, different electrode arrays were compared in terms of sensitivity [21]; apart from IDE arrays, there also exist serpentine electrodes (SRE), spiral electrodes and meandered electrodes, all represented in the figure below.

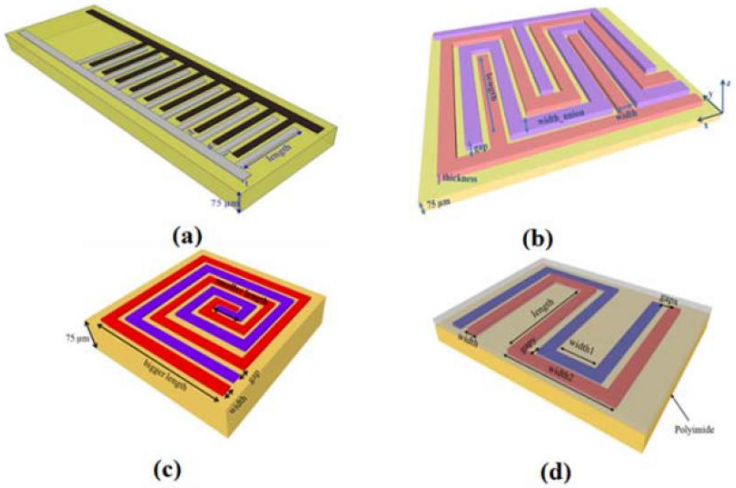

Figure 4. Different electrode configurations of capacitive sensors: (a) interdigitated electrodes, (b) serpentine electrodes, (c) spiral electrodes and (d) meandered electrodes. [21]

Using five capacitors of each configuration, capacitances were measured at 1 MHz as a function of the relative humidity [21]. Measurements were normalized with respect the area of the sensors and calibration curves were compared. Results show that the highest sensitivity was obtained by SRE, followed by spiral electrodes, IDE and meandered electrodes. Although SRE and spiral electrode configurations present better sensitivity values, their design is more complex than IDE and meandered electrodes [21]. In the end, the choosing of the sensor is always a balanced decision between the pros and cons.

In line of these studies, different biological factors have been detected by changes in the conductivity of the medium measured. One way of detection consists of measuring impedance changes caused by the detection of a specific molecule by a captured antibody in the electrode spacing (S) and the posterior attachment of a secondary antibody modified by a gold nanoparticle [4]. The idea behind this design is that the bounded gold nanoparticle will disrupt the electric field around the electrodes leading to a decrease in the impedance. In this proposed model, the target biomolecule will make the bridge between the modified GNP antibody and the electrode surface.

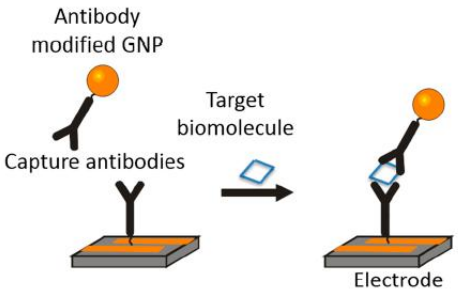

Figure 5. Schematic representation of biomolecules detection using IDEs [4]. An antibody is placed in the spacing of the IDE. Under the presence of a target molecule, a secondary modified antibody will bind to the molecule and the primary antibody, disrupting the electrical field of the IDE [4].

Yet impedance measurements are not restricted to biomolecules; the presence of organisms like bacteria is also possible and researched. Detection of two different bacterial strains (*Staphylococcus and Pseudomonas*) were achieved by the measurement of relative changes in the solution of antibody functionalized IDEs [3]. Antibody functionalized polysilicon IDEs has also been used to perform selective detection of live *Escherichia coli* cells by the measurement of relative changes in the solution [22].

The last achievement is the aim towards this work is being done. Starting by the base, the characterization of the IDE and the proposal design is directed to a 3D culture implantation for the real-time detection of different cellular phenomena, including the further detection of bacteria.

3. Planning and development

3.1 Bachelor Thesis structure

As extracted from the previous paragraphs, this Bachelor Thesis pursued two main objectives.

Firstly, it pursues the characterization of a novel interdigitated sensor (IDE) printed over a flexible substrate by inkjet printing technology. This first characterization was done using just the IDE and culture media.

Next step in the characterization process focused on monitoring the HaCaT cell culture by means of these sensors. Prior to culture the epithelial cells over the IDE, an experimental assay was performed to assess the cell viability of the cells on the sensor. Once it was proved that the IDE was biocompatible, the experiments involving *in vitro* cellular culture started.

During the experimentation, the main problems encountered were the necessity of reusing the sensors to have three different repetitions of each condition and the excessive amount of noise at low frequencies. Furthermore, for the testing of the new batch of sensors that arrived in June 2019, a change in the impedance/phase analyzer equipment was done.

In the first point of this Bachelor Thesis, an overall introduction of the topic has been done, introducing a possible scenario in which interdigitated sensors are able to provide real-time responses for the monitoring of the wounds in severe burned patients.

Point 2 summarizes the development of the interdigitated sensors of the last two decades applied to the cellular detection, as well as their evolution into different configurations and the main biologically relevant milestones achieved. This point, point 3, states the main objective of the following Thesis as well as the regulatory framework followed.

Point 4 covers the Materials and methods part of this work. It is subdivided into six main parts. *Proposed plan, requirements and restrictions* (4.1) explains the strategy followed in this work, as well as the issues encountered along the path. *Experimental assays* (4.2) details the theoretical principles of the assays performed. *Fabrication and*

implementation of the IDE (4.3) covers the first objective of this work, including the manufacturing process of the sensor, the different implementation of the tested IDEs and the empirical data processing. *Characterization of the sensor applied to cellular culture* (4.4) details the second goal of my project, from the cell viability to the experiments involving cellular cultures.

Solution design. Interdigitated sensor implementations for models 2 & 3. Noise reduction experiments (4.5) takes into account all the knowledge learned from the characterization of model 1 and proposes a design for the new sensors (model 2 and 3) as well as a new implementation to reduce noise at low frequencies, that is the main drawback of this Bachelor Thesis. Lastly, *Data processing: statistical analysis, formulae and table* (4.5) explains the test performed to assess the cell viability results, as well as all the mathematical equations employed to analyze the empirical data obtained.

Point 5 contains the results obtained both in the characterization of the sensor (model 1) itself (5.1) and in the application of the sensor to cellular culture (5.2). *Cell visualization* (5.3) details the results obtained from the visualization techniques that have served to ensure that the detected electrical change corresponded with a real biological phenomenon: cellular attachment. Finally, the results of the solution design are included in section number 5.4, where a noise reduction experiment was carried out with the new equipment to check if the new implementation was suitable for the next year.

. Point 6 discuss the overall results obtained from this work, both for the characterization of the sensor itself (6.1) and in the application of the sensor to cellular culture (6.2), as well as the checking by means of optical visualization that the electrical change corresponded with the cellular attachment phenomenon (6.3). This part ends with the general conclusions of the overall work to be applied to the final solution design of the new models (6.4) and some conclusions regarding the new implementation proposal.

Finally, Further studies at point 7 summarizes the next steps to be followed in this project with the new models proposed. Point 8 contains the bibliography used in this work and in the annexed (point number 9), both the budget and the project schedule can be found.

3.2 Regulatory framework

All the experiments described were performed respecting the required safety rules. The experiment involving HaCaTs-GFP cells were performed in the Level 2 biological contention laboratory of Carlos III University of Madrid. The clothing and basic PPEs were constituted by a lab coat and protection gloves (latex or vinyl). The lab coat was mandatory and exclusive in the laboratory area. Sterile chamber ensures the proper culture conditions and avoided contamination of the sample.

Regarding the impedance-phase analyzer, the equipment used has been designed in accordance with EN6 1010 “Safety requirements for electrical equipment for measurement, control and laboratory use”. Furthermore, safety precautions contained in the user manual were followed during all the experiments [23].

4. Materials and methods and solution design

4.1 Proposed plan, requirements and restrictions

4.1.1 Electrical impedance definition. Measurements methods

Cellular cultures under the presence of a small current create a resistance towards the current flow due to the insulating properties of cell membrane [24]. By means of impedance spectroscopy, this cellular impedance, also known as bio-impedance, will be measured with the aim of obtaining information about some relevant biological phenomena.

In the following work, cells will be seeded directly over the sensor, with the electrodes in direct contact with the medium. By applying AC voltage to the IDE, it is expected a change over time due to the presence of the cells. The empirical data will be fitted to an equivalent electrical circuit to understand the influence of each circuit's element in the response obtained.

4.1.2 Non-faradaic detection: equivalent circuit analysis

In this work, non-faradaic detection is the operation principle by which the results are being understood and interpreted. Therefore, the changes in the overall ionic medium are expected to induce a change in the double layer capacitance of our sensor.

The electrical equivalent circuit commonly used for non-faradaic impedance biosensors consists of an electrolyte resistance also known as solution resistance (R_s) in series with a charged transfer resistance (R_{ct}) that accounts for the leakage current in parallel with a constant phase element (CPE) which represents the double layer capacitance [25].

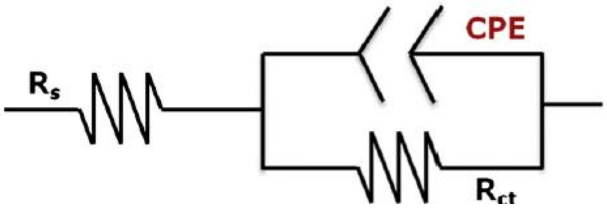

Figure 6. Schematic representation of the equivalent circuit of non-faradic impedance spectroscopy [25]. Here, R_s stands for the solution resistance, whereas R_{ct} stands for the transfer resistance. CPE represents the constant phase element that describes the double layer response of a real capacitor [25].

The equations of the equivalent circuit elements are defined as: [26]

$$R_s = \frac{1}{k}\frac{l}{A} \quad (1)$$

Where:

k ≡ conductivity of the solution

l ≡ length in which current is carried

A ≡ area in which current is carried

$$R_{ct} = \frac{RT}{\eta F i_o} \quad (2)$$

Where:

R ≡ gas constant

T ≡ temperature

η ≡ overpotential ($E_{app} - E_{DC}$)

F ≡ Faraday's constant

i_o ≡ exchange current desity

and

$$Z_{CPE} = \frac{1}{(jw)^{\alpha} Y_o} \quad (3)$$

Where:

$Y_0 \equiv C \equiv$ capacitance

α ≡ empirical constant from the Nyquist arc

It must be remarked that the CPE is not a capacitor. CPE is a non-intuitive circuit element that is used to interpret the response of the double layer of an imperfect or real capacitor. It behaves at described in equation 3, where alpha is an empirical constant that ranges from 1 to 0. When alpha is equal to one, it means that the phase element is behaving as an ideal capacitor, whereas when this parameter equals zero, it means that its behavior is purely resistive [27].

Its use in this work is justified by the Nyquist plots presented in the results section (see 5.2.3). Nyquist plots are used in this work as polar plots to assess the behavior of the sensor in terms of its equivalent circuit elements. These polar plots represent the imaginary part of the impedance versus the real part of the impedance, in such a way that each point in the diagram correspond to the modulus of the impedance in a given frequency.

As the curves described in this work are not perfect circles but arcs that can be identified as the depressed semicircle models, the constant phase element serves here to fit the circuit and find a real physical meaning to the circuit parameters [28]. Furthermore, cellular behavior cannot be modeled nor explained through pure resistive or capacitive elements. In order to approach to the biological phenomena, constant phase elements are needed.

The proposed Nyquist plot for those materials in which kinetic and diffusion factors play a role in the polarization process was first described as by Randles in 1947 [29]. This equivalent electrical circuit is known as Randles cell and is modeled as shown in figure 7. Here, the solution resistance is obtained by the first point cutting the x-axis, whereas the charge transfer resistance is the result of manually completing the semicircle and obtaining the second x-axis point resulted from the intersection of the semicircle with the x-axis.

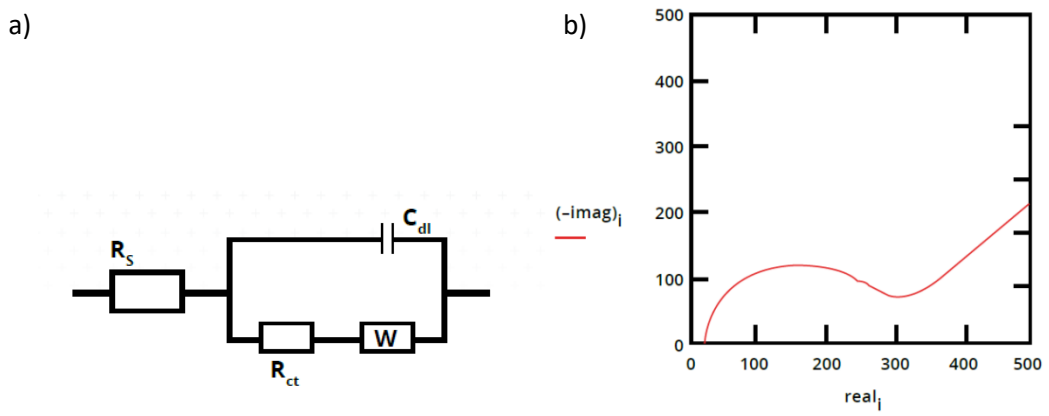

Figure 7. Schematic representation of a) Randles' equivalent electrical circuit and b) its characterization in terms of its resulting Nyquist plot. This circuit has been proposed to characterize the materials in which kinetic and diffusion factors play a role [29]. The arbitrary values that the different circuit elements take are the following: the Warburg coefficient, σ, is assumed to be about 150, Rs = 20 Ω Rct = 250 Ω and Cdl = 40 μF.

Although in this work the cellular phenomena is not expected to perfectly mimic the Randles circuit and its corresponding Nyquist plot, as capacitors must be substituted by constant phase elements, it has served us as a starting point in the understanding of the expected behavior a system including diffusion and kinetic parameters may have.

4.1.3 Interdigitated sensors: description and operation principles

IDE is the selected electrode configuration for this work. Interdigitated sensors consist of two set of electrodes with a comb shape placed in the same plane, parallel to the substrate. These set of electrodes have a number of individual fingers, with a width D and a length L, interlocked but separated a distance S. Figure 8 details the schematic representation of such interdigitated sensors.

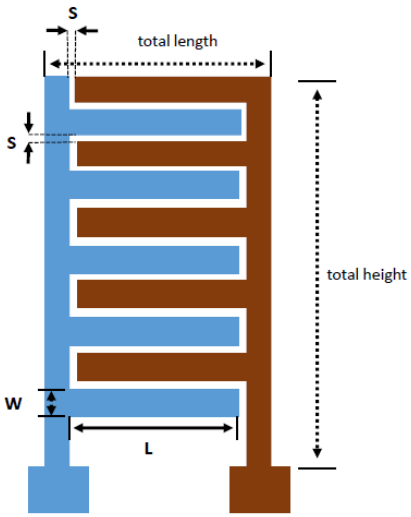

Figure 8. Schematic representation of an IDE, where S stands for spacing, W for width and L for length. IDEs normally present two sets of electrodes with individual fingers placed on the same plane.

In presence of a voltage, either AC or DC, an electric filed is created between its fingers, also known as digits. The principle of operation of the sensor is the same as the conventional parallel-plate capacitor: this fingerlike periodic pattern of parallel in-line electrodes is used to build up the capacitance associated with the electric fields penetrating into the material or sensitive coating [30]. The disruption or alteration of such electric field, by either cells or even specific target biomolecules, is the basis of detection.

The basic equation of the capacitance in a parallel-plate capacitor is shown below.

$$C = \varepsilon_o \, \varepsilon_r \frac{A}{d} \quad (4)$$

Where ε_o stands for the vacuum permittivity, ε_r is the relative permittivity of the material connecting the plates, A is the electrode's surface area and d is the distance between the plates

The equation of the interdigitated sensor has been defined as it is stated in equation 5:

$$C = \eta\varepsilon \frac{lt}{d} \quad (5)$$

In this case, η represents the number of fingers, ε is the permittivity of the sensitivity coating field, l is the length of the interdigitated electrodes, t is the thickness of the electrodes and d is the spacing between the electrodes [19].

Unlike the conventional parallel plate capacitor, in which the electric field lines are linear and enclosed by the electrode plates, the key point for understanding the IDE's physical principle is that the electrical field generated is also influenced by the electric field lines coming from the outside of the electrode plates. These lines, known as fringing field lines, are bended rather than linear and must be rigorously taken into account when modeling the IDE in 3D.

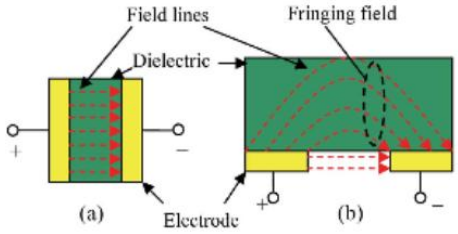

Figure 9. Comparative in the electric field lines between a) a parallel plate and b) an interdigitated capacitor [31]. As it can be appreciated, in the case of an IDE the field lines are linear at the electrode base but also bended from the top of one electrode to the other.

For the same given spacing between the electrodes (S), the higher the frequency, the higher the height of the electric field and therefore the higher the penetration depth of the field into the sample. Consequently, the sensing volume is changing with frequency, which makes the final measurement more unspecific. In addition, for the same frequency, the smaller the spacing between the electrodes the higher the electric field lines and therefore the deeper the field penetration into the sample.

4.1.4 Requirements

There are three main requirements the IDE sensor must fulfill for the *in vitro* approach desired in this work.

- In the first place, in order to build a suitable model for future *in vivo* implantation, and for performing the required *in vitro* tests, it was necessary to work with a biocompatible sensor. For a sensor to be biocompatible it must present the ability of providing an appropriate host response once implanted in a

living organism. For first *in vitro* measurements, this biocompatibility was tested using human epithelial cells (see point 4, materials and methods part, and specifically 4.4.1 for the cell culture description).

- To continue, and in order to measure impedance and associate these measurements with cellular phenomena, the IDE sensor must be able to detect changes in response of cellular confluence. If there did not exist significant differences between our sensor design with and without cells this design must be re-evaluated.

- Finally, as this design proposal has been thought to deal with a 3D cell culture model, electrodes must be completely attached to the surface of the sensor and passivated to it.

4.1.5 Restrictions

The following issues were encountered during the performance of this project.

- For the solution design, although according to bibliography a reduction from 30 μm to 10 μm would increase the sensitivity around 69% [19], gap spacing between electrodes could not be made lower than 10 μm due to limitations in the fabrication process. The minimum feature size achievable by the manufacturer was of 300 μm. Considering that the HaCaT cells' size is approximately of 20-25 μm, a smaller sensor could have been suitable for detecting smaller changes. However, having our device one order of magnitude bigger than the object under study avoids granularity effects of the measurement. It allowed studying the cell culture dynamics as an array instead of individually detecting changes produce by a single cell.

- More sensors would have been needed to complete the experiments of model 1, as well as for the statistical analysis of models 2 and 3, but a second set of sensors has not been available until very late in this course and thus they could not been used for this bachelor thesis.

4.2 Experimental assays

4.2.1 Cell viability assay. Alamar Blue

A material is considered biocompatible if both the function and the structure of the biological system in contact with it remain unaltered. A biocompatible sensor must present the ability of providing an appropriate host response once implanted in a living organism, supporting the cell proliferation and growth.

In order to check this, cell viability assays must be carried out as a first step of any *in vitro* experiment. There are several ways of measuring cell viability, that is, the cellular capacity to proliferate on a given environment. The most commonly used compounds include MTT, MTS, XTT and WST-1 [32]. In this work, Alamar Blue is the chosen assay. Alamar Blue is a bioassay that incorporates a fluorometric/colorimetric growth REDOX indicator based on detection of metabolic activity, that is, it takes advantage of the reducing capacity of cells to check cellular viability [33]. This REDOX indicator compound is named resazourin. Resazourin enters into the cells in its non-fluorescence form (blue), where it is reduced to resorufin, which is fluorescence (red) [32]. The fluorescence emission can be then correlated with respect several testing days to check whether the material of interest supports cell viability (see 4.4.2 Cell viability assay for the description of the procedure followed and 4.5 Data processing,, for more information about the processing of the results).

The main reason this assay was chosen is because it is not toxic and it does not interact with the normal cell metabolic activity as other tests such as MTT, therefore it allows working with the same culture during the 6 days the test lasted.

4.2.2 Electric Cell-Substrate impedance sensing. AC characterization

The main goal of this work is to associate changes in capacitance and impedance with cellular phenomena, that are expected to alter the impedance response of the medium, as it has been graphically represented in figure 10. Keeping this in mind and considering previous studies dealing with *in vitro* impedance characterization models, AC characterization over a wide range of frequency and time was first performed.

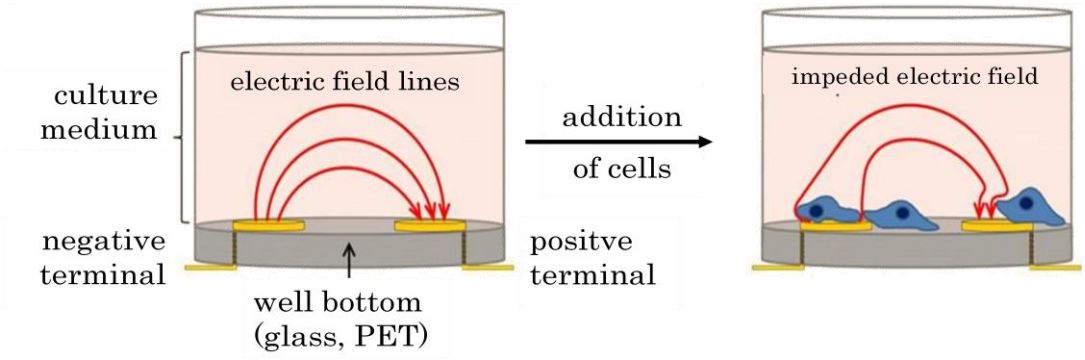

Figure 10. Schematic representation of how the electric field lines are altered under the cellular presence. It can be appreciated that, upon the addition of cells, the previous parallel electric field lines between the electrodes are impeded by the cells attached over the electrodes.

The idea of using a big frequency range when taking the measurement was to cover in a first moment a wide range of frequencies to check at which points the information obtained became more important. Once these critical frequency points were founded, it will be possible to focus on them analyzing the changes with time. The two different amplitudes chosen were below the threshold by which epidermal cells will be damaged, as the HaCaT resting potential is, according to bibliography, of -27 ± 4 mV [34]. Difference between media volume was selected just in order to analyze if the amount of volume over the sensor affects significantly the measurement (point 5.1 explains this characterization in detail).

Moreover, the use of a wide time range (36 hours) would allow the detection of specific processes, as well as the association of these processes with the real cellular phenomena. In order to verify that the changes in the impedance curves correspond to cellular specific phenomenon, samples were observed with the Scanning Electron Microscope (SEM) at different times. Once this first characterization was done, the time range will be readjusted to focus on the critical hours.

Finally, to analyze the impedance measurements obtained both in magnitude and in phase, Zview [35] software was used for the equivalent electrical circuit fitting of the impedance data. This way, all the elements values were obtained for each of the measurements in time. Each of the elements of the circuit were analyzed individually, and their variations plotted at the Results section (5).

4.2.3 Amperimetric sensing. DC characterization

DC current detects the conductivity between the electrodes, that is, detects just the real part of the impedance. This means that the frequency effects over the penetration depth into the sample are avoided, making this time a more specific measurement of impedance when compared with the AC characterization.

Theoretically, the presence of cells on the electrodes would alter the conductivity of these electrodes.

4.3 Fabrication and implementation of the sensor

4.3.1 Fabrication of interdigitated electrodes by inkjet printing

Inkjet printing is a direct and additive fabrication technology that is nowadays employed to produce micro-patterns. It is a low-cost technology and requires low-temperature microfabrication on flexible substrates. Furthermore, ink consumption is reduced by using drop-on-demand process, in which the delivery is precise and controlled [36].

The process essentially consists of the ejection of inks in a fixed quantity from a nozzle through a sudden, quasi-adiabatic reduction of the chamber volume via piezoelectric action. In response to the application of an external voltage, the chamber is contracted causing a liquid drop to eject from the nozzle. The ejected drop falls due to the action of gravity until it gets to the substrate, spreading into it and surface tension aided flowing along the surface. Then, it dries through solvent evaporation [37].

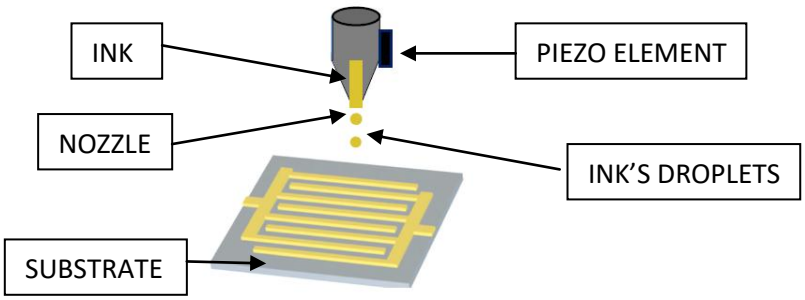

Figure 11. Schematic representation of IDE fabrication using inkjet printing technology. Droplets are ejected through the nozzle by the actuation of a piezoelectric element and the droplet falls to the substrate under the action of gravity [37].

Recent studies have shown that drop spreading and final printed shape strongly depends on the viscosity of the ink, which is proportional to the molar mass of the material chosen as ink. Furthermore, the material concentration affects the final dried drop diameters' height [36]. All these factors must be carefully taken into account in order to achieve a proper resolution.

4.3.2 Interdigitated sensor implementation for model 1

First sensors employed consisted on an array of electrodes of semiconductor ink over PET substrate, printed by inject printing technique. The width of these electrodes was of 130 µm, with a spacing of 260 µm.

With the first aim of characterizing the interdigitated electrode sensors (IDEs), two different implementations were tested. In both cases IDEs were attached to the bottom of a cell culture well (ThermoScientific Petri dish, Ø 35mm) using biocompatible high vacuum grease (Dow Corning). A copper adhesive tape (3M ™; 1181-12) was used for external cable connections. Figure 12 shows this implementation.

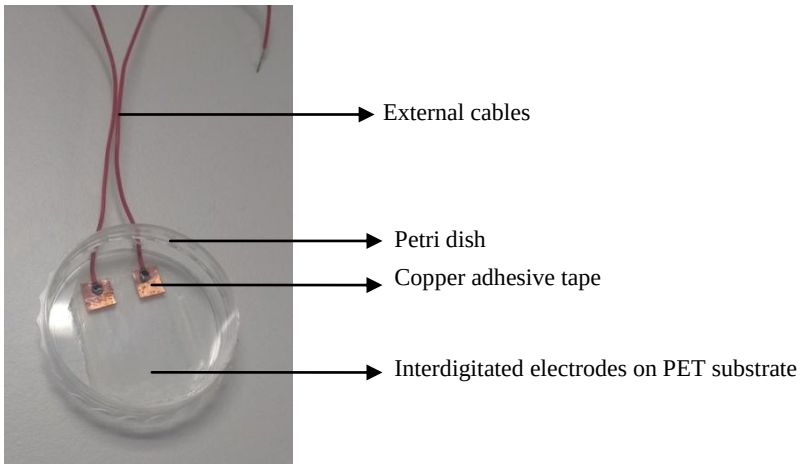

Figure 12. IDE model 1, first implementation. It consisted of attaching the IDE to the bottom of the Petri dish using a biocompatible adhesive (Dow Corning). A copper adhesive tape was used for the external cable connections.

Second implementation included PDMS ring surrounding the IDEs' structure. The rationale behind this was that cells might slide to the edges of the sensor when they were cultured on the plate.

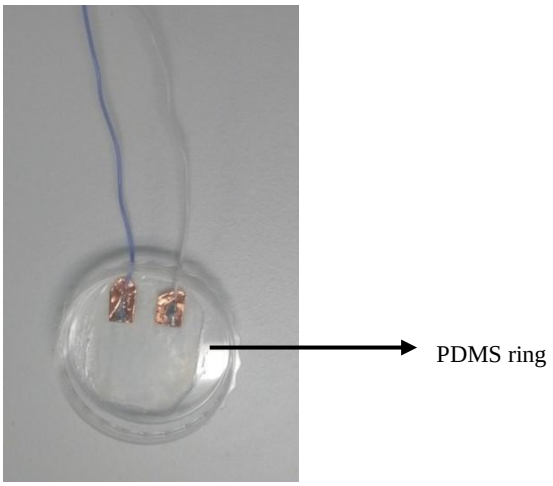

Figure 13. IDE model 1, second implementation using a PDMS ring surrounding the IDE. As in the first implementation, the IDE was attached to the bottom of the Petri dish using a biocompatible adhesive (Dow Corning). A copper adhesive tape was used for the external cable connections.

The second implementation was discarded (see the results and discussion section, 5.1 and 6.1 respectively, for further information), and the first model was reproduced two times more for having the required variability in the cell-substrate impedance measurements. There was another extra setup employed for the picoamperimeter characterization, setup 4, with exactly the same implementation that the one shown in figure 14.

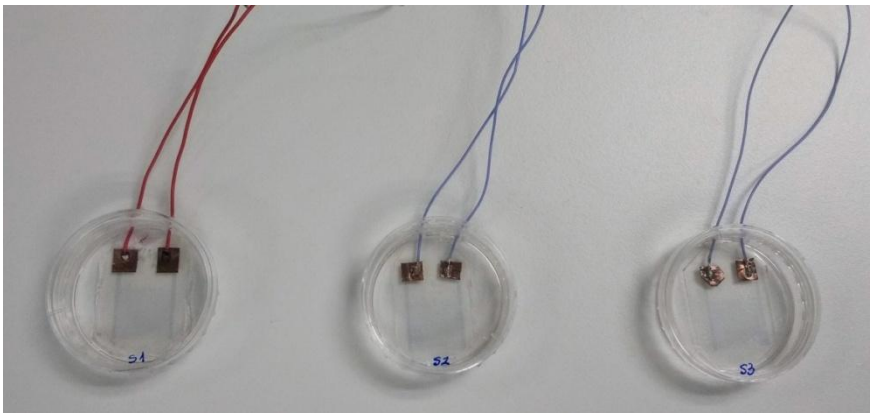

Figure 14. IDEs following model 1: named setup1, setup2 and setup3. The three of them were implemented in exactly the same way, attaching the IDE on the Petri dish plate by means of a biocompatible glue and using a copper adhesive tape to make the external cable connections. At least three repetition of each experiment must be done in order to obtain proper statistically coherent results.

4.3.3 Proposed equivalent circuits: without and with cells

Before running the experiments involving cellular presence, the characterization of the IDE itself was performed by adding just culture medium over the IDE.

IDEs were measured using the culture medium without cells and 20 mV of amplitude, inside the bioreactor. This first measurements were best fitted using the following electrical circuit, coinciding with the equivalent model proposed for non-faradic detection using IDEs sensors:

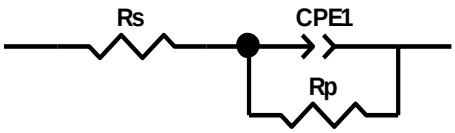

Figure 15. Schematic representation of the equivalent non-faradic circuit for cellular pre-attachment. Here, R_s stands for the solution resistance, whereas R_p stands for the transfer or polarized resistance and CPE represents the constant phase element.

The circuit corresponds to the non-faradic most employed equivalent circuit, in which R_s is associated with the solution resistance, R_p is the polarized or transference resistance and CPE is the double layer capacitance.

This circuit was therefore the starting point when the experiments with cells started. The main goal of this project is to detect impedimetric changes associated with the cellular presence on and between the electrodes. Thus, it was expected that the equivalent circuit would change once the cells had reached the electrode surface at the bottom of the Petri dish. Two different models were proposed and tested to study the cellular attachment from the electronic perspective:

- **Circuit 1: Rp affecting all the circuit components in series with Rs**

Figure 16 shows the model proposed in a first instance to argue this change in terms of cellular presence:

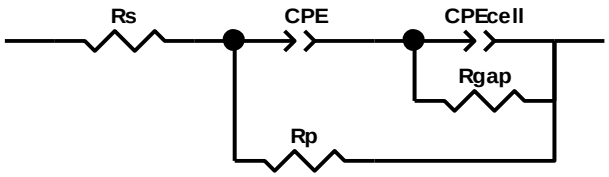

Figure 16 Schematic representation of the first proposed equivalent non-faradic circuit for cellular attachment. In the same way as before, R_s stands for the solution resistance, whereas R_{ct} stands for the transfer resistance and CPE represents the constant phase element. CPE-cell stands for the capacitance behavior of the lipid bilayer of the epithelial cell, whereas the R_{gap} represents the current conduction only due to the extracellular matrix (ECM). Here, the addition of the time element due to the cellular presence is made parallel with the polarized resistance of the previous circuit without cells.

The rationale behind it is that the addition of cellular culture over the sensor surface must affect the double layer capacitance generated in such a way that at least one more time constant element would be taken place into the equivalent circuit. Therefore, CPE-cell would stand for the capacitance behavior of the lipid bilayer of the epithelial cell, whereas the R_{gap} represents the leakage current that will traverse the cell from the electrode without passing through the cell, that is, the current conduction only due to the extracellular matrix (ECM).

Moreover, the charge transfer or polarized resistance, R_p, is designed to be in parallel with both the CPE and the time cellular time constant. In this way, the current would be able to follow two different paths: depending on the frequency, it could traverse both the IDE's own constant phase element and the cellular one or it could just pass through the charge transfer resistance without even reaching the double layer capacitance of the sensor. Solution resistance, R_s, is in series with the rest of the circuit and its value is expected to be related with the volume of the solution.

- **Circuit 2: Rp in parallel with CPE1, but in series with the rest of the circuit elements**

Figure 17 represents the second electrical circuit proposed to understand the cellular presence on the interdigitated sensor.

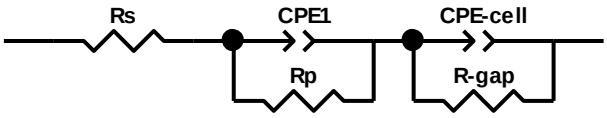

Figure 17. Schematic representation of the second chosen equivalent non-faradic circuit for cellular attachment. In the same way as before, R_s , stands for the solution resistance, whereas R_{ct} stands for the transfer resistance and CPE represents the constant phase element. CPE-cell stands for the capacitance behavior of the lipid bilayer of the epithelial cell, whereas the R_{gap} represents the current conduction only due to the extracellular matrix (ECM). Here, the addition of the time element due to the cellular presence is made in series with the previous circuit without cells.

In this case, the transference resistance does not interfere with the cellular attachment; the theoretic necessity of another constant time element is maintained: CPE-cell remains in parallel with the ECM resistance. This second circuit is supported by the scientific community and still makes sense from an electronical point of view.

Here, there is only one path for the current, it necessarily would traverse first the sensor's constant phase element and then the one due to the cellular presence, independently of the employed current. The solution resistance, R_s, is in series with the rest of the circuit and its value is expected to be related with the volume of the solution in the same way as before.

4.4 Characterization of the sensor in cellular cultures

4.4.1 Cellular culture

HaCaT cell line is an immortal keratinocyte cell line transformed from adult human skin. These cells are widely employed in the research field due to their ability of proliferate and differentiate *in vitro*.

The HaCaT-GFP cell line is created by the transfection of GFP encoding vector into the HaCaT cells. GFP is a fluorescent protein allowing the visualization of cell nuclei when exposed to light in the blue to ultraviolet light range.

4.4.2 Cell viability assay

The in vitro cytocompatibility test employed was the alamarBlue® Assay. As said before, this assay is an indicator of cell metabolic activity and viability just by measuring the dye indicator resazurin (REDOX indicator); viable cells reduce resazurin into resorufin generating a fluorescent signal correlated with the proliferation activity.

Changes in the fluorescent expression of the dye are observed both in absorbance and in fluorescence. In absorbance spectroscopy, the measurement is performed at a given wavelength of light excitation. In fluorescence spectroscopy, the light absorbed by the sample has a different wavelength that the light emitted, due to the mechanism of relaxation of electrons, and what is measured is the emitted light of the sample.

To perform the cell viability assay, the HaCaTs-GFP cells were cultured on 1x1 mm inside p24 Petri dishes (Ø 12 mm) in culture medium (DMEM supplemented with 10% fetal bovine serum (FBS) and 2% Ab). The initial density was 40% of confluence, which corresponds to $55.76 * 10^4$ cells/area.

Cells were incubated overnight under 5% CO_2 and 37ºC conditions. The day after, the cell viability assay was taken as day 1.

4.4.3 Impedance spectroscopy and conductivity experiments

As a starting point, two different setups were created with model 1 sensors: one assembly consisted of the sensor glued on the bottom of the culture plate whereas the other one also incorporated a PDMS ring to ensure the localization of cells inside the sensor. Before setup duplication both assemblies were compared.

These two assemblies were measured with the impedance gain-phase analyzer (Impedance gain-phase analyzer SI 1260) at room temperature. 2 mL of culture medium (90% DMEM, 10% FBS, 5% Antibiotic) were added over the sensors and impedance modulus and phase were recorded at a testing amplitude of 20 mV. The fit with the selected equivalent circuit, previously discussed, were performed and plotted with the measured data.

Once one of the assemblies was discarded (see results and discussion, 5.1 and 6.1 respectively, for more details), the analysis of impedance spectroscopy was

performed using the assembly without the PDMS. To continue with the setting, 2 mL of culture medium were added to the IDE, inducing two different perturbations of AC voltages signals: at 5 and 20 mV, with 0 mV of DC voltage, in the frequency spectrum from 10kHz to 0.1 Hz. After analyzing the results, the 20 mV amplitude was selected to perform the following measurements (see results and discussion, 5.1 and 6.1 respectively, for more details).

To continue, the setups were covered with 2 mL and 1.5 mL of culture medium at room temperature and using the bioreactor. As before, the impedance spectroscopy analysis was performed by using the impedance phase/gain analyzer.

Next step was to perform the cell-substrate impedance spectroscopy. In order to create a controlled *in vitro* environment, these setups were placed inside a bioreactor (constant temperature of 37℃, same humidity and CO_2 as in the human body) and three different conditions were applied to the sensor:

- 2ml of culture medium (90% DMEN, 10% FBS, 5% Antibiotic) without cells, as a control for a better appreciation of the effects of culture in terms of impedance.
- 2ml of the same culture medium with HaCaTs-GFP at 80% of confluence ($156.8 * 10^4$cells/area).
- 2ml of the same culture medium with HaCaTs-GFP at 40% of confluence ($15.6 * 10^4$cells/area).
- In all these cases the measurements were taken with the impedance phase/gain analyzer each 2 hours during 36 hours.

Due to the shortage of sensors, the setups were reused for the three conditions measurements. The protocol used before reusing the sensors was the following:

1. Media aspiration
2. PBS washing (twice)
3. Add 1mL of Trypsin and incubate for 10 min.
4. PBS washing of the Trypsin (3 times).
5. 15 min of UVA light inside the chamber
6. Cellular addition to the plate and impedimetric measurements restart.

An inverted microscope with phase contrast (LEICA CKX41) with an incorporated cell culture station was used to check visually that HaCaTs-GFP were proliferating during these 36 h. Pictures were also taken each 2 h.

Figure 18 shows the complete setting of the impedance spectroscopy measurements, which includes the sensor as well as the analyzing equipment.

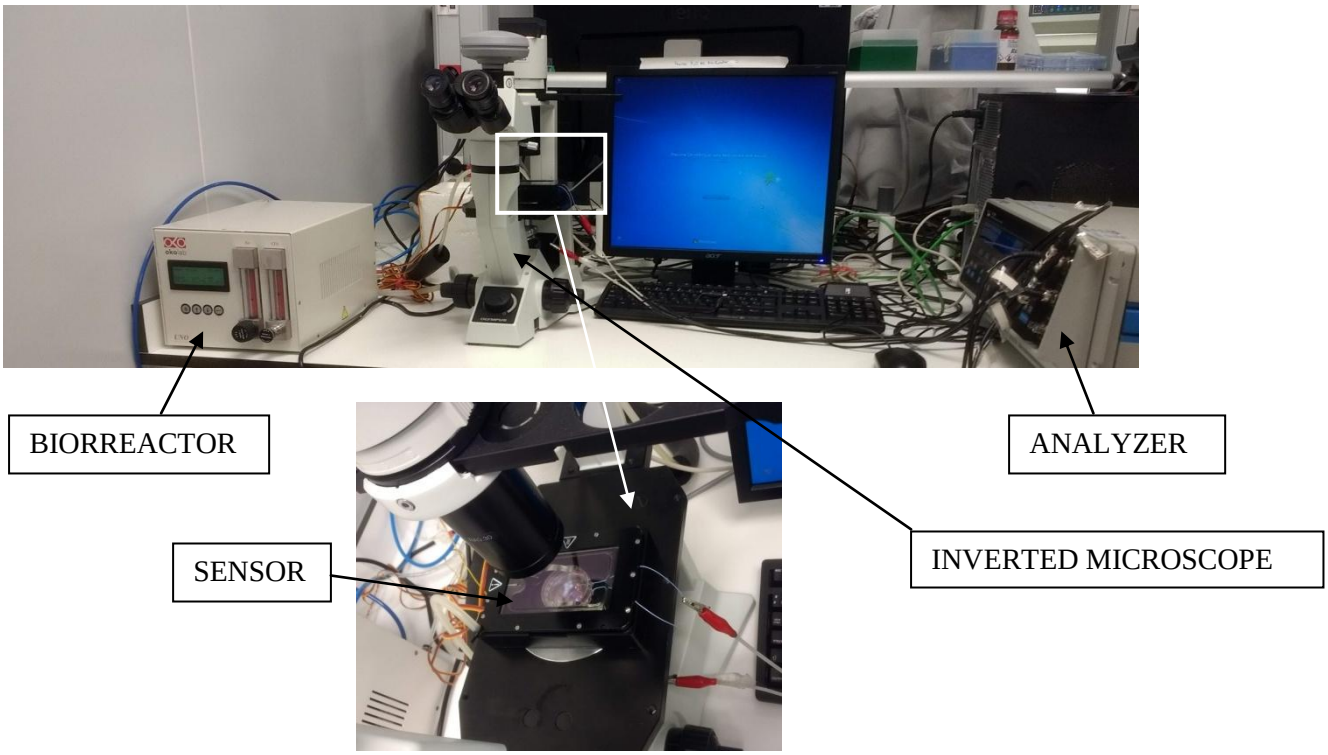

Figure 18. Impedance spectroscopy assembly. HaCaT cells were seeded over the IDE in the incubator. The connections with the impedance/phase analyzer were done with the copper cables outside the bioreactor and the inverted microscope was used to take some control images of the process.

Once these experiments were performed, the setups were reused to be measured with the picoamperimeter (KEITHLEY 6487) at room temperature (2 mL, 20 mV of amplitude) and then with the setups placed in the bioreactor, repeating one condition as before:

- 2ml of culture medium (90% DMEN, 10% FBS, 5% Antibiotic) without cells, which would serve to us as a control for a better appreciation of the effects of culture in terms of impedance.

Figure 19. Picoamperimeter measurements assembly.The IDE was connected with the picoamperimeter by means of its copper cables.

The original idea consisted of introducing the cellular culture phenomenon as it was done when dealing with alternating current; however, the results obtained testing the IDE without cells (see 5.1 for a detailed explanation) forced us to stop using reused sensors for the following experiments. As explained in the restriction section, the shortage of the sensors paralyzed this research line.

The picoamperimeter was connected in series with the sensor, as shown in the figure 35. The voltage was measured from 0 V to 1 V, with a step of 0.1 V.

4.4.4 Cell shape and sensor visualization using inverted microscope and SEM

There were three different hypotheses to be solved by means of directly visualization of the cells on the sensor:

- The effect of the induced electric field on the cellular culture: it was expected that the selected electric field did not induce a massive cellular death or apoptosis.
- The attachment of the cells on the electrode fingers: it was expected that the cells were able to attach to the whole sensor equally.
- The biological relevant mean, if any, of the electrical detection by means of the IDEs.

As PET is not fully transparent, visualizing the cells over the sensor supposed a challenge at first. Images obtained from the inverted microscope with phase contrast were not as clear as expected, specially due to the generation of small bubbles proceeding from the generation of an electrical field during the experiments (see Results

section, point 5, and specifically point 5.3, for further information). This led us to try to visualize the cells with the scanning electron microscope (SEM).

In order to observe the morphology of the cells attached to the sensor surface with the SEM, the electrical field was needed to be removed from the equation, as there were no possibility of inducing the electric field while visualizing with the microscope.

To prepare the samples, cells were seeded at 40% of confluence over the sensors during different times before fixing them (12 h, 18h, 22h and 40h). Each of the samples, including the cells seeded on the Petri dish were fixed using the same protocol.

In the first place, the samples were washed with NaCl (0.9% in distilled water). Then, Glutaraldehyde (2.5% in distilled water) water fixing was performed, leaving the samples with the solvent for 30 minutes. The samples were rinsed with PBS three times and then it was dehydrated with 1 mL of ethanol (30%, 50%, 70% and 100% each 20 minutes). The samples were left to dry inside the cabin and then stored at 4℃.

To continue, pieces of approximately 0.5 cm of diameter were selected, surrounded with a conductor tape and placed on Aluminum stubs. As cells are not conductive, samples were first treated by gold sputtering technique (LEICA EM ACE200) for 90 seconds. Then, the samples placed on the Aluminum stubs were introduced in the SEM chamber and visualized (PHILIPS XL 30) and images were taken at different magnifications (from 20μm to 500μm) and with 15 KV of penetration depth.

4.5 Solution design. Interdigitated sensor implementation for models 2 and 3. Noise reduction measurements

After performing the characterization experiments with model 1 and detecting their main flaws, the following two model designs were proposed, taking into account the printing limitations of the manufacturer.

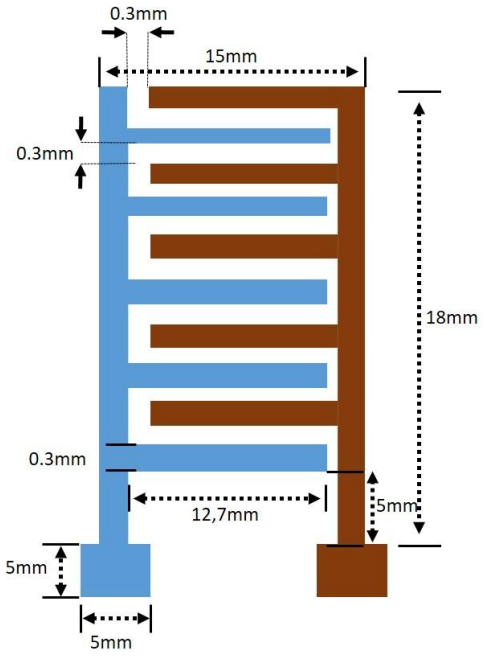

Figure 20. Schematic representation of desired design for models 2 and 3. Both models 2 and 3 consist of the same array of comb-shape electrodes with a length of 18 mm, a gap of 0.3 mm and a spacing of 0.3 mm.

The difference between both models relies in the conductor inks; model 2 was still created using a metal ink whereas the ink of model 3 was made of a semiconductor polymer (SU8) in order to enhance the biocompatibility of the sensor.

Furthermore, noise problematic that model 1 presented especially in the frequency range between 0,1 Hz and 10 Hz was approached by designing a new implementation. Instead of using a copper adhesive tape for creating the contact between the cables and the electrodes, a conductor resin (Epoxy H2O) was proposed to ensure a proper attachment to the IDE. Furthermore, a tape made of Kapton and Silicon (Tesa 51408) was proposed as a passivator.

a) b)

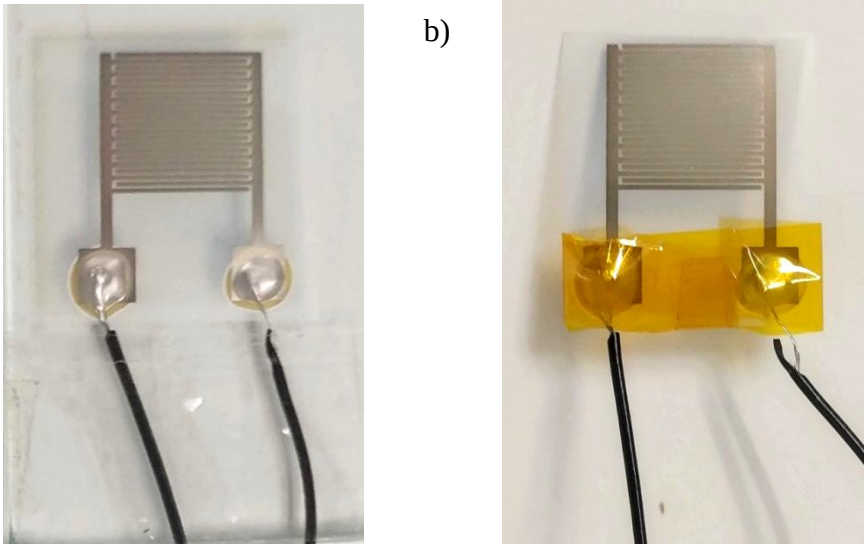

Figure 21. Model 2 with the new implementation. Image a) shows the welding of the IDE's electrode and the copper cable with the resin EpoxyH2O, b) shows the passivation achieved by using the Kapton tape.

As explained before, the new batch of sensors arrived too late to proceed with the characterization of the two new models. Nevertheless, model 2 was used to test the new implementation proposed with the new impedance/phase analyzer (ISX-3mini).

In order to check whether this new implementation achieved a noise reduction, two different experiments were done using just the culture medium (without cells) under controlled conditions by means of the bioreactor.

- First experiment consisted of testing the response in magnitude of both the old implementation and the new one, by means of impedance spectroscopy.
- Second experiment consisted of testing the effect of the passivator over the welded IDEs by means of impedance spectroscopy. In order to do this, the same IDE was measured in magnitude before and after the passivation

4.6 Data processing: statistical test, formulae and table of nomenclature

For the analysis of the data corresponding with the Alamar Blue assay, the ANOVA statistic test was performed using the SPSS Statistics program. The ANOVA test performs an analysis of variance that provides information about whether the results are significant, that is, if there exists or not a difference between the results obtained at different conditions.

In the case of the cytocompatibility measurements, as the experiment consists in three different measurements (day1, day2, day3) repeated three times, the ANOVA was performed as model of repeated measurements. If the p-value obtained is bigger than 0.05 the equality of variances hypothesis cannot be rejected, and therefore there are not significant differences between the measurements taken.

Regarding the way in which the empirical data has been processed and analyzed, the following equations were applied to find a relation between measurements with cells and without cells.

- Nyquist plots (representation of the imaginary part of Z with respect to its real part):

Complex impedance equation:

$$Z = R + jX$$

Module:

$$|Z| = \sqrt{R^2 + X^2}$$

Phase:

$$\theta = \arctan\frac{X}{R}$$

Reactance equation:

$$X = |Z|sin\theta$$

Resistance equation:

$$R = |Z|cos\theta$$

- Variations within the different elements of the circuit:

$$\Delta CPE = \frac{|CPE - CPE_0|}{CPE_0}$$

$$\Delta Rs = \frac{|Rs - Rs_0|}{Rs_0}$$

Regarding the characterization of the IDE in terms of the impedance and conductivity, all the experiments shown in the characterization of model1 had been repeated three times, one time per setup, in order to have the proper variability to obtain statistically relevant measurements. However, when dealing with model 2, as the sensors arrived too late to start with the experiments, the only characterization made was in terms of the noise reduction, and it was not repeated three times but one.

Results presented for model 2, are not sufficient, as they lack of a proper repetition (at least 3 IDEs should have been made of each type of condition). They are presented here as a proof of concept of the improvement in the new implementation regarding the major problem of this Bachelor Thesis, that is the huge source of error affecting the measurement, especially at low frequencies (from 0,1 to 10 Hz).

Finally, all the graphs with their respective standard errors were created with OriginPro v9.

- Table of nomenclature:

Table 1. Table of nomenclature

Nomenclature	Parameter
C	Control plate with just cells and DMEM medium
C-PET	Control PET substrate with cells and DMEM medium
C-ink	Sensor material: PET + ink + cells
Point 1	Frequency point: 0.25119 Hz
Point 2	Frequency point: 0.794333 Hz
Point 3	Frequency point: 25.11886 Hz
Point 4	Frequency point: 2511,886 Hz
S1	Setup 1
S2	Setup 2
S3	Setup 3
S4	Setup 4
40%	40% of cellular confluence
80%	80% of cellular confluence
CPE	Double layer capacitance
Rs	Solution resistance

5. Results

5.1 Characterization of the sensor

5.1.1 Impedance spectroscopy. Comparative between PDMS ring assembly and without PDMS ring assembly

The first objective of this Bachelor Thesis was to characterize the sensor itself in order to make an implementation that would allow us to apply the IDE to a 2D in-vitro cellular environment.

With this aim in mind, two different assemblies were created and compared by means of impedance spectroscopy: one sensor was glued to the Petri-dish plate directly whereas a PDMS ring surrounded the other. As explained in the Materials and methods part, culture medium was used to cover the sensors and the impedance/phase analyzer was employed to induce an electric field and record the impedance response.

Figure 22 presents the impedance phase and magnitude values of both the PDMS ring implementation and the sensor without the PDMS ring. From this graph, it can be appreciated a change in the modulus of the magnitude impedance values when the PDMS ring was introduced in the setup. This is not an important problem, as the values will be later normalized. However, the phase becomes more affected and unfitted with the PDMS ring.

This qualitative study was sufficient to check that the PDMS ring over the IDE had an influence over the measurement and especially over the phase, that probably affected the sensor performance. Therefore, the implementation with the PDMS ring was discarded and the following experiments were made using the implementation consisting of the IDE itself glued on the Petri-dish plate.

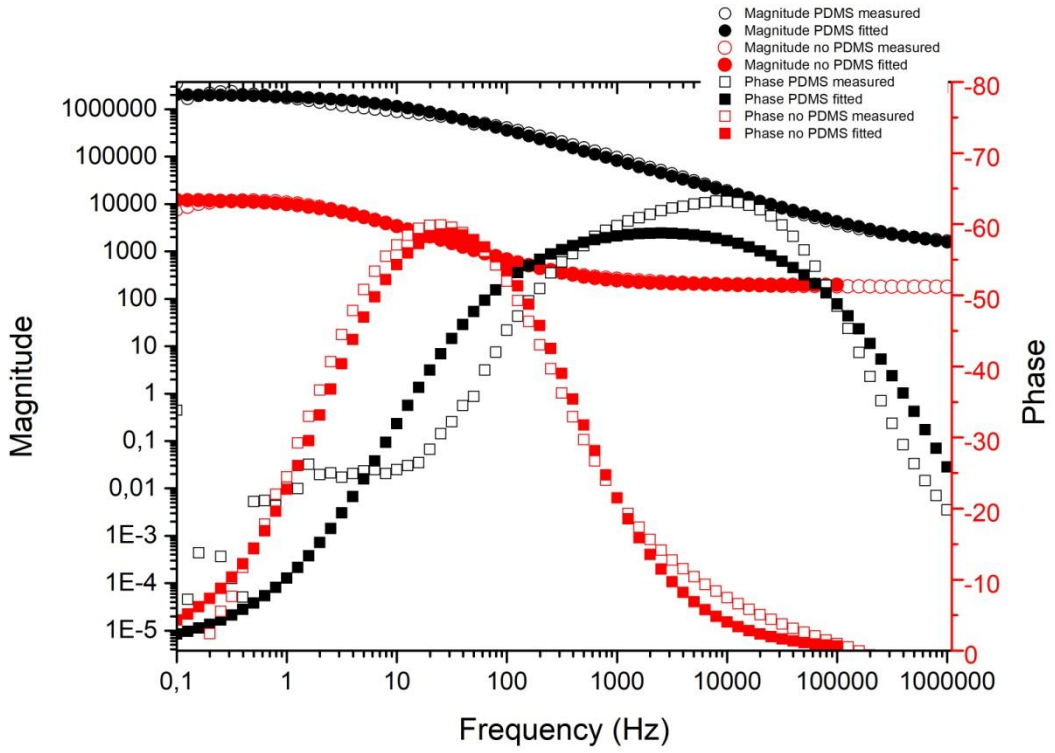

Figure 22. Comparison in both magnitude and phase of total impedance between with PDMS (hollowed black dots) and without PDMS (hollowed red dots) assemblies. Filled dots, black and red respectively, represent their electrical equivalent circuit fitting. It can be appreciated how the phase became more distorted and unfitted in the PDMS assembly.

5.1.2 Impedance spectroscopy. Comparative between 20 mV and 5 mV of amplitude

The curves shown in figure 23 represent the modulus of the magnitude and phase measured at 5 mV and 20 mV. Especially at low frequencies, it can be clearly distinguished that noise affects more the lower amplitude of 5 mV than the 20 mV amplitude. Setup 3 presents a higher scattering than setups 1 and 2; this is explained by the fact that these measurements were taken in an uncontrolled environment (see next point).

Even in this worst-case scenario of noise, it can be appreciated how the 20 mV amplitude measurements are less affected. In addition, according to bibliography, 20 mV is closer to the resting potential of HaCaT cells [34], but still it is a safe tension value to induce the electric field without damaging the cells by altering their resting potential. This experiment served us to continue the following experiments using a voltage of 20 mV.

a)

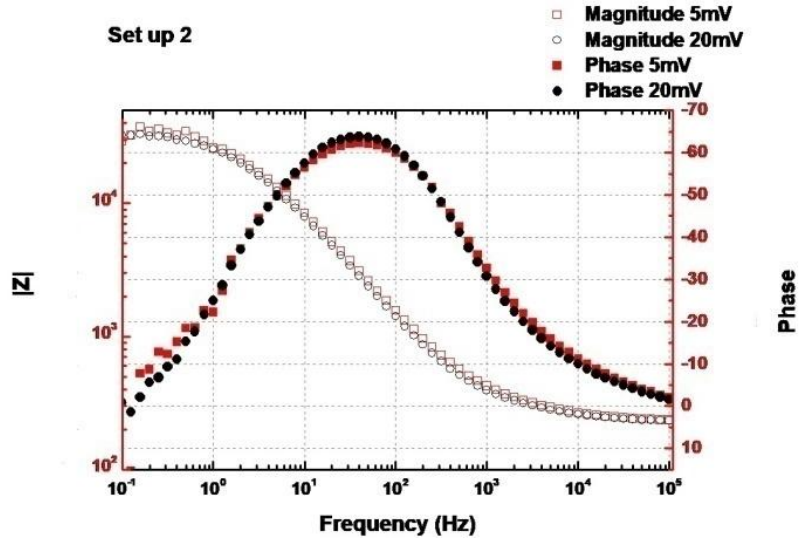

b)

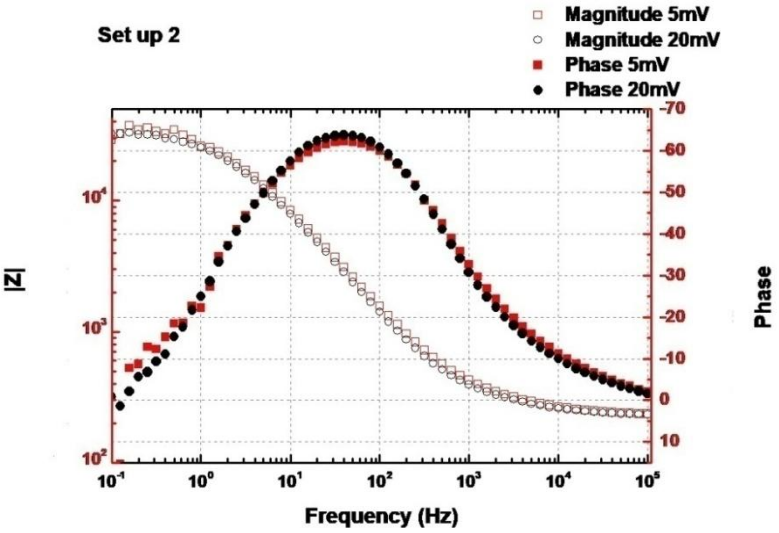

c)

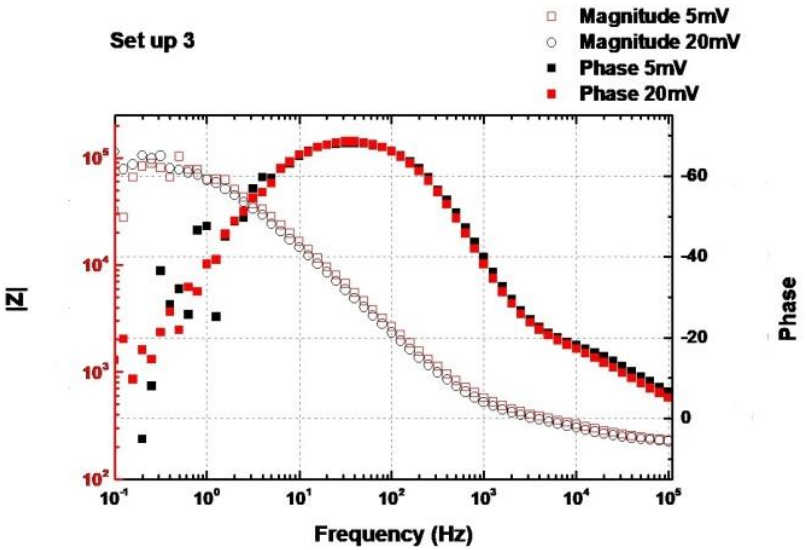

Figure 23. Comparison in both magnitude and phase of total impedance between the 5mV and the 20mV amplitude measurement in a) setup 1 b) setup 2 and c) setup 3. The most perceived difference relies in the comparison between phases. When inducing a 5 mV change, the noise affects the phase at lower frequencies much more than the curves inducing 20 mV.

5.1.3 Impedance spectroscopy. Comparative between conditions: with and without the bioreactor

The first aim in order to characterize the IDE was checking the variability of the different setups and then finding a relation between medium volume and impedance measurements. In order to do this, measurements of 20 mV in amplitude were done for the three setups in both uncontrolled conditions (without the bioreactor) and controlled conditions (with the bioreactor).

Furthermore, as in theory the solution resistance, R_s, has been defined as the parasitic resistance coming from the solution in which the sensor is embedded, two different volumes were used in order to prove this hypothesis:

- Without the bioreactor: setup1 has 2 mL of medium over the sensor, whereas setups 2 and 3 have 1,5 mL.
- With the bioreactor (controlled conditions): the three setups have 2 mL of medium.

According to the legend shown in figure 24, black points represent the different setups in uncontrolled conditions, that is, at room temperature without the bioreactor. Between the three of them, there exists a clearly appreciated variability, even between setup 2 and setup 3, which have exactly the same volume of medium over the sensor. By looking at the black points, it is clear that the sensors must be placed inside the incubator for the two different cellular confluences, but also for the controls without cells.

Red points represent the three setups covered by 2 mL of medium and placed inside the bioreactor. From them, it can be appreciated that the variability decreases as expected: red points are closer to each other when compared with black ones. However, higher variability is still presented at low frequencies. This is associated with noise interference and its reduction will be pursued in the following work (see further discussion and conclusions).

Concerning the association of the measurement with the solution resistance, R_s, the magnitude values of the impedance measurements obtained in controlled conditions are closer to the first setup containing 2 mL of medium than to the other two containing 1,5 mL. For the bioreactor measurements, all the setups contained 2 mL of culture

medium; as the first setup was the only one containing this same volume of media, it can be inferred that there exists a relation between the volume of media over the sensor and the starting point of the measurement obtained.

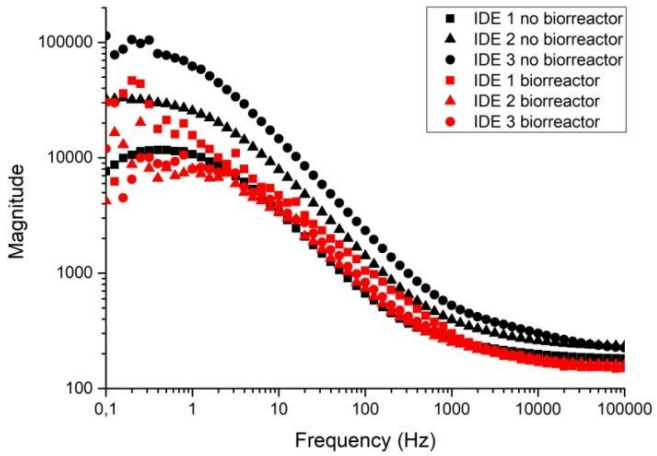

Figure 24. Comparison in magnitude of the impedance between the three setups, with the bioreactor (red points) and without the bioreactor (black points). It can be appreciated that the red dots are closer to each other, whereas in the case of the black dots, the variability between setups increases. Moreover, the three setups of the bioreactor contained 2 mL of medium, and they are closer to the setup 1 (IDE 1 no bioreactor), which contained exactly the same medium volume. In the case of the other two setups (IDE 2 and IDE 3 no bioreactor), they both contained 1,5 mL of medium, but they are far from each other under uncontrolled conditions. This proves that the controlled condition imposed is behaving as expected and that the solution resistance is directly related to the amount of volume over the IDE.

5.1.4 Equivalent electrical circuit fitting: without cells (control)

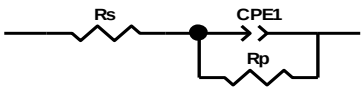

First step in order to find an appropriate equivalent circuit for the sensor was to propose a control equivalent circuit, that is, an equivalent circuit representing just the effect of the solution resistance over the IDE in terms of impedance. As detailed in the Materials and methods section, the proposed equivalent circuit for the controls consisted of a solution resistance (R_s) in series with both the constant phase element (CPE) and the polarized resistance (R_p).

To check that this control equivalent circuit was suitable for our sensor, the three control measurements from the three setups were fitted using the previous electrical circuit, in the frequency range from 0,1 Hz to 1E+07 Hz. The control measurements

were made by means of impedance spectroscopy analysis and consisted of 2 mL of cellular culture medium over the IDE. Figure 25 shows the process using setup 2 as an example. As in the control measurements the cellular phenomenon cannot take place, the circuit should remain well adjusted with the first proposed equivalent circuit for all the measurements. Figure 23 shows the results for two different time moments (t =2 h and t = 34h).

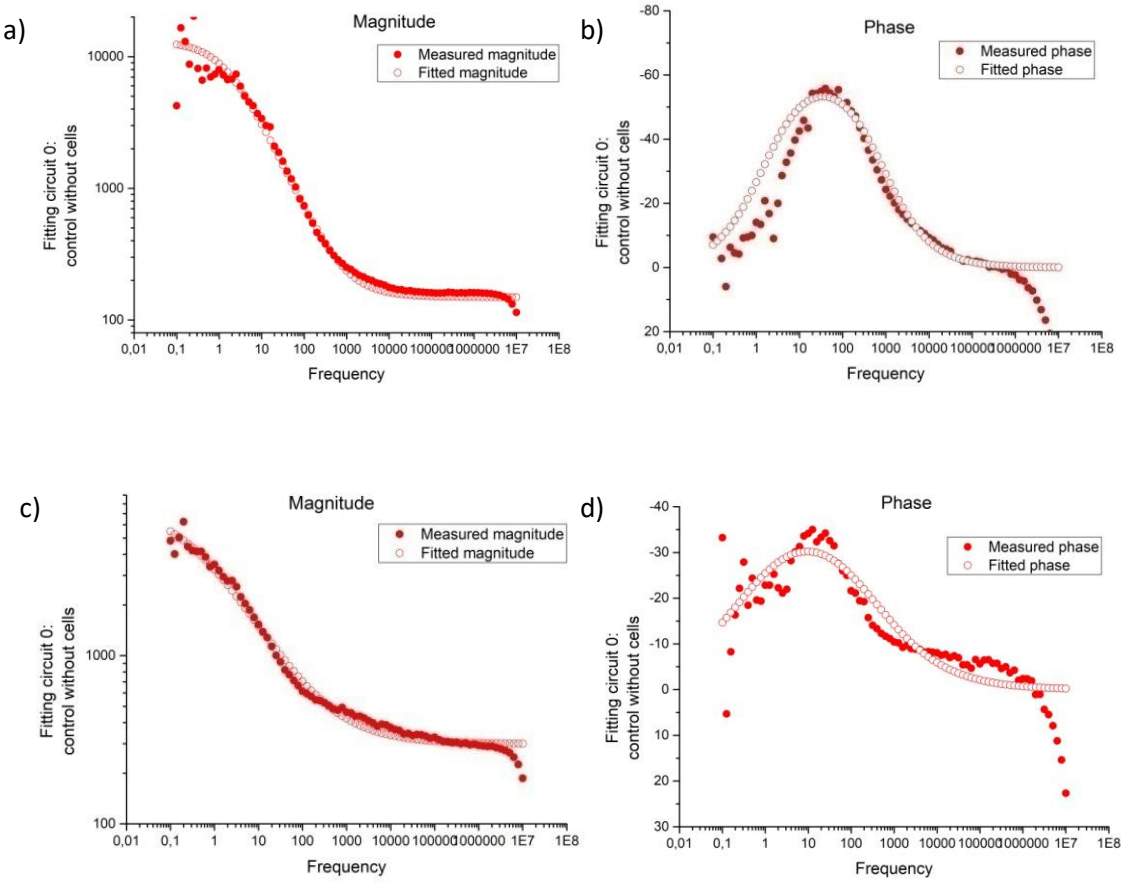

Figure 25. Equivalent circuit fitting of setup 2 at t =2h (above) and t =34h (below), without cells in both a) and c) magnitude and b) and d) phase. Red dots correspond with the measured empirical data, whereas white points correspond with the theoretical values employed to fit this data with a theoretical equivalent circuit. In both cases, the magnitude is best fitted than the phase. Nevertheless, it is clearly appreciated that the quality of the fitting is not compromised over time. The electrical circuit of the control, therefore, does not change in time. Noise reduction to guarantee a better fit is the next step.

Table 2 contains the numerical percentage errors values that confirm this hypothesis for the three setups: in fact, after 34 h the percentage of errors of the equivalent circuit elements has been reduced rather than increased.

Table 2. Evolution of both the values and the errors (%) of all the equivalent circuit elements of the control measurements of the three setups at t = 2 h and t = 34 h. There has not been an increase in the errors with respect to time. The electrical equivalent circuit applied to the control measurement without cells remains the same along the 36 hours that this experiment lasted.

	Rs	CPE-T	CPE-P
Setup 1			
t=2h	117,9	2,97E-05	0,70
Error (%)	6,714	8,4605	2,48
t=34h	121	7,98E-05	0,39
Error (%)	5,10	4,38	1,85
Setup 2			
t=2h	132	1,24E-05	0,80
Error (%)	3,378	11,40	2,74
t=34h	276,8	1,95E-05	0,40
Error (%)	1,97	7,53	2,86
Setup 3			
t=2h	130,6	1,84E-05	0,72
Error (%)	5,40	11,84	3,1202
t=34h	235,6	3,94E-05	0,58
Error (%)	2,21	7,27	2,25

The polarized resistance in the three setups increases with respect to time, achieving a magnitude more than ten times the value of the initial control measurements (it started in values up to 1E+05 and ended in values of the order 1E+15) and presenting errors up to 40%. The electrical implication of such big values is that the current will flow just through the constant phase element of the circuit instead taking the path between the electrodes. Therefore, its role in the equivalent circuit is negligible and that is the reason why instead of being presented in the table it is commented.

5.1.5 Picoamperimeter measurements

In the first place, sensors were characterized by means of impedance spectroscopy, by applying an AC voltage to the IDEs. IDEs were first tested without cells, adding just

culture media, as it has been shown before. Then, these same IDEs were reused and tested with cells under controlled conditions by means of a bioreactor.

Once these impedance spectroscopy experiments finished, the characterization of the sensor in terms of its conductivity was aimed. This characterization would have been achieved by means of the picoamperimeter, which induces a DC voltage and record the conductivity response of the IDE. Mimicking the same procedure done with the impedance spectroscopy experiments, the sensors were tested without cells by the addition of just culture medium.

The curve shown in figure 26 presents the following flaw: the measurement does not stabilize as expected when the bioreactor was introduced. It can be appreciated how the measurements of S3 and S4 differs more than reasonably expected when the conditions are controlled.

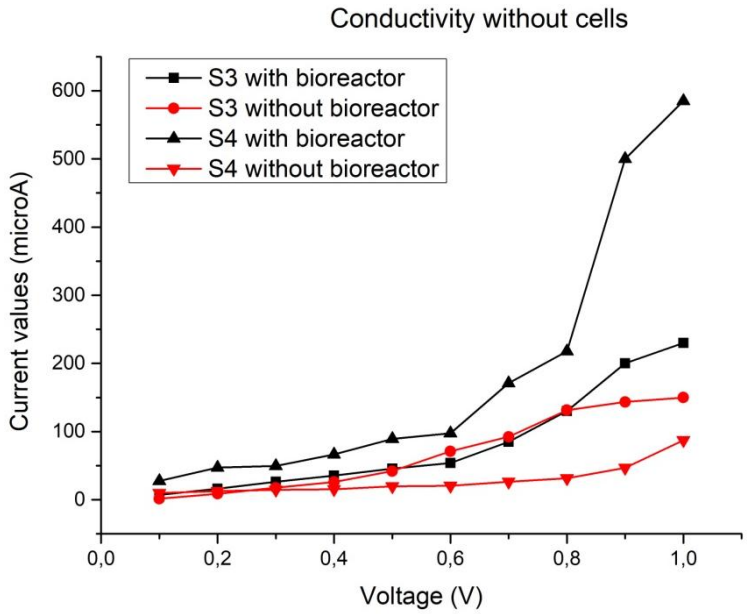

Figure 26. IDE's response under the presence of a DC current. This figure represents an inconsistency, since measurement does not stabilize as expected when the bioreactor is introduced (black points) when compared with the measurements performed without the bioreactor (red points). Instead of stabilizing, it can be appreciated how S4 and S3 differ more than reasonable.

One AC impedance measurement was performed to check whether the non-faradic capacitive behavior of the device was still observed. The result was that the response of the sensor has been lost. The lack of more sensors paralyzed this research line. However, the result is shown here as it served us to realize that the lifetime of our IDEs was not limitless. The main hypothesis that was being considered was that the

sensor had been deteriorated due to their repetitive reuse during the impedance spectroscopy measurements both with and without cells.

5.2 Cell-substrate impedance spectroscopy

5.2.1 Cell viability test

Before starting the experiments involving 2D *in vitro* cellular cultures, the Alamar Blue cell viability test was performed to assess the cellular viability and correlate this viability to the cellular proliferation on the sensor.

Both the fluorescence and the absorbance graphs presented in figure 27 show the amount of reduction with respect to the control for days 1, 3 and 6. These graphs are an indicator of how similar the cellular activity of days 1, 3 and 6 is with respect to the control well, in which cells were seeded over a Petri dish plate. Two different substrates were tested: the PET substrate itself (C-PET) and the PET substrate with the metallic ink printed on it (C-ink). Graphically, it can be appreciated how both the PET and the PET containing the metallic ink do not differ more than 10 % from the control in any case, being their average over the control in all the cases for the substrate containing the metallic ink.

Differences in both graphs may be explained by the fact that the reduced form of alamarBlue® is highly fluorescent [33]; therefore, small changes in reduction will be detected with a higher sensitivity with the fluorescent approach rather than with the absorbance one.

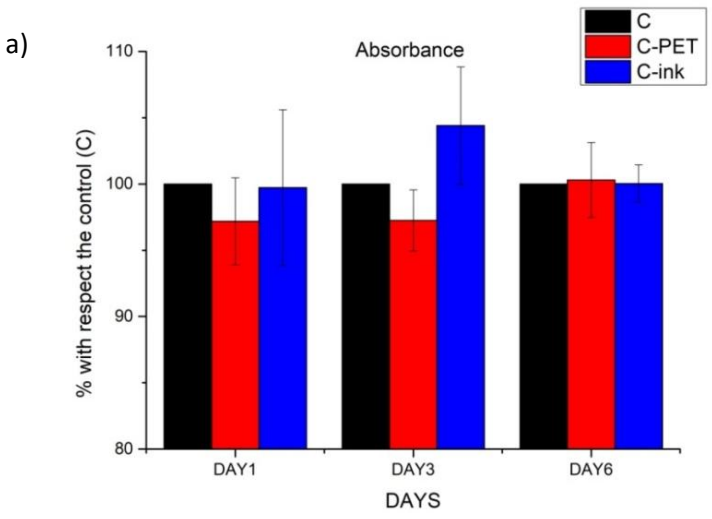

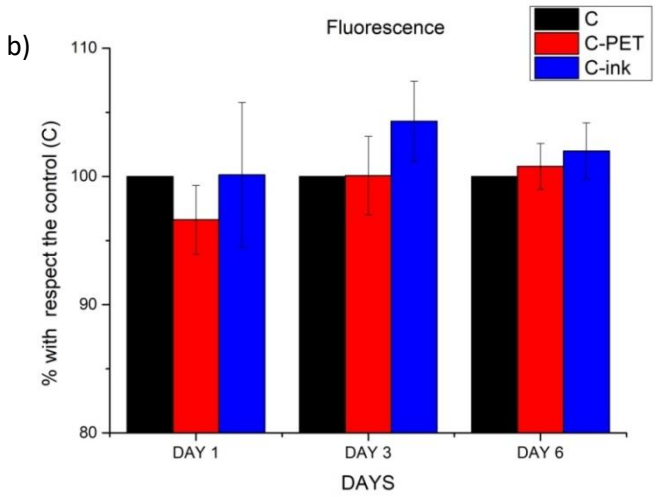

Figure 27. Cytocompatibility results both in a) absorbance and b) fluorescence percentage of reduction with respect the control (C). It can be appreciated how PET substrate and PET containing the metallic ink substrate support proliferation in a way very similar to the control during the six days that the experiment lasted.

ANOVA statistical test for repeated measurements was made to assess whether there exists significant differences between the cellular activities of the substrates with respect to the control. Table 3 presents the p-values obtained by running an ANOVA test of repeated measurements with cell absorbance and fluorescence values. Both absorbance and fluorescence values show a p-value bigger than 0.05.

Table 3. ANOVA-test results. p-values of both the PET and the PET containing the metallic ink substrates are bigger than 0.05, which means that the null hypothesis cannot be rejected. In this particular case, the null hypothesis was that the proliferation was equal in these substrates with respect to the control. As the p-value is bigger than 0.05, it cannot be stated that the cellular activity of both substrates differ from the activity of the cells seeded over a Petri-dish.

	p-value PET	**p-value PET+ink**
Absorbance	0,951	0,507
Fluorescence	0,859	0,400

In addition to these graphs, the fluorescence values of the three different conditions were normalized with respect day 1. Figure 28 show that the cellular activity of PET and PET containing the metallic ink substrates was similar to the control in days 1, 3 and 6. With this new graph, it is also assessed if the cellular activity increases with time with respect the first measurement. Cellular activity is associated with proliferation, thus an increase of the activity necessarily means that cells are proliferating over the substrates.

In figure 28, this proliferation activity can be observed. As expected, there is an increase with respect day 1 metabolic activity in the three different conditions.

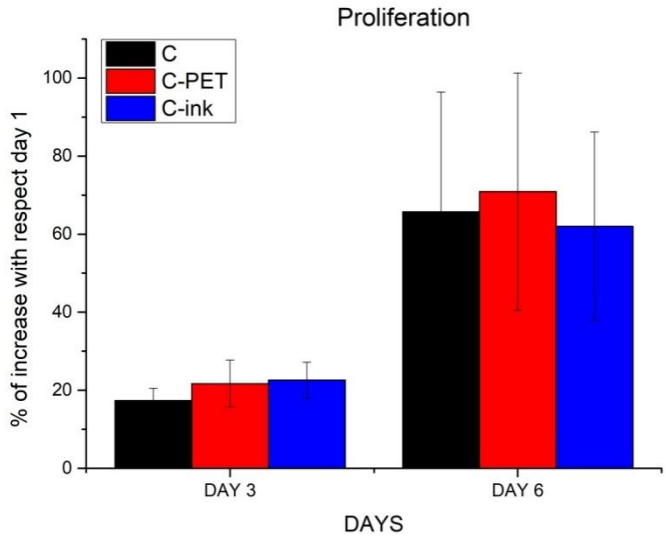

Figure 28. Normalized percentage of reduction with respect day1. It can be appreciated that, although the errors at day 3 are quite big, in both days the cellular activity has increased with respect the first day and therefore proliferation is being supported by the three substrates

5.2.2 Study of stability

First thing it was checked when working with the impedance analyzer in controlled conditions (with the bioreactor) was whether the measurement was effectively performed, that is, whether the signal was stable and not buried by the noise recorded. With that goal in mind, four points were selected; point 1 and point 2 were in a range before the cut-off frequency and point 3 and 4 were in a range after this frequency.

It can be observed in figures 29 and 30 how the first two points are more affected by the noise than points 3 and 4, specifically noise can compromise the measurements made on the frequency range from 0,1 Hz to 10 Hz. Nevertheless, noise did not affect the phase critically in either of them. In all the graphs, the magnitude is within a consistent value range: the variation is only of one order of magnitude. Regarding the phase, it has a variation around 90 degrees, as theoretically expected from the behavior of a capacitor, specifically it falls around 60 degrees in all of the graphs.

From all these remarks it was considered that the following measurement can be performed using the selected equipment and sensors. Noise at low frequencies would be

one of the cons the following designs would try to correct (see next discussions for further information).

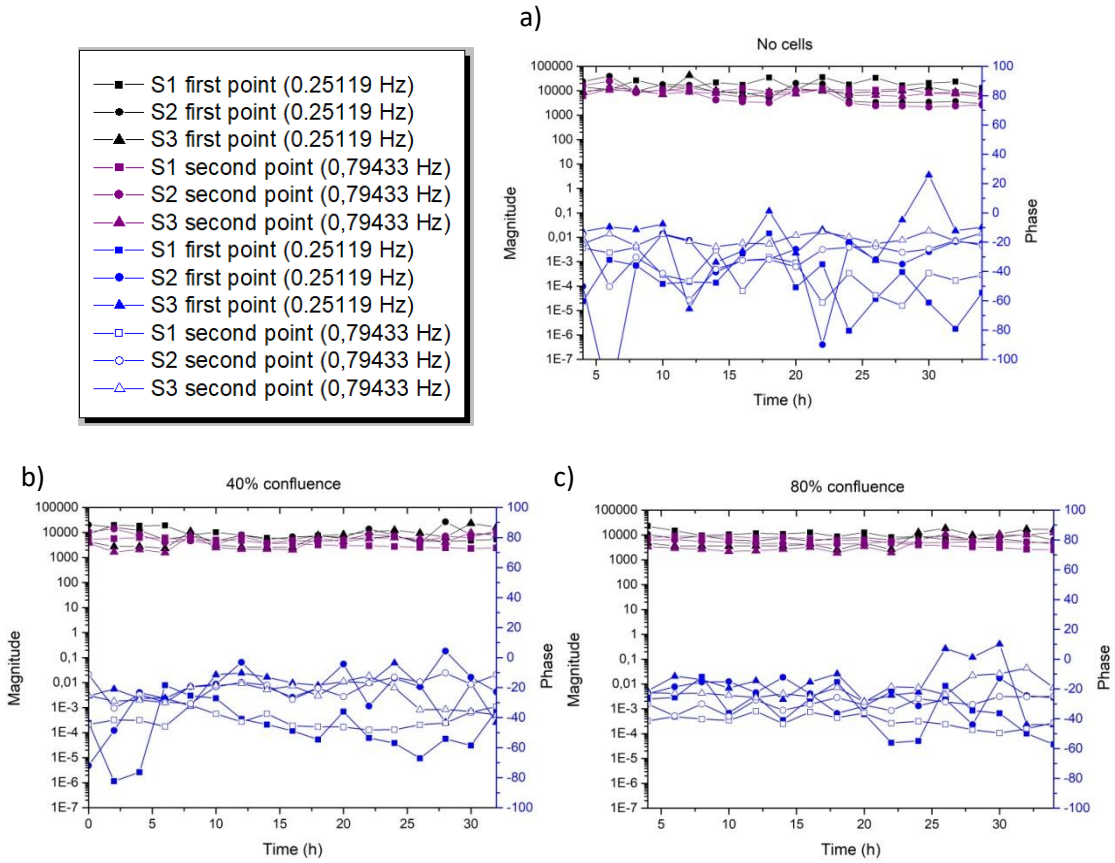

Figure 29. Study of consistency of points 1 and 2 (both below the cut-off frequency) in the three setups in conditions a) without cells b) 40% of confluence and c) 80% of confluence. At low frequencies, the noise is affecting the measurement in a higher way compared to higher frequencies (points 3 and 4). However, this noise does not affect the phase critically. Magnitude variation is around one order of magnitude, whereas phase variation is around 60 degrees.

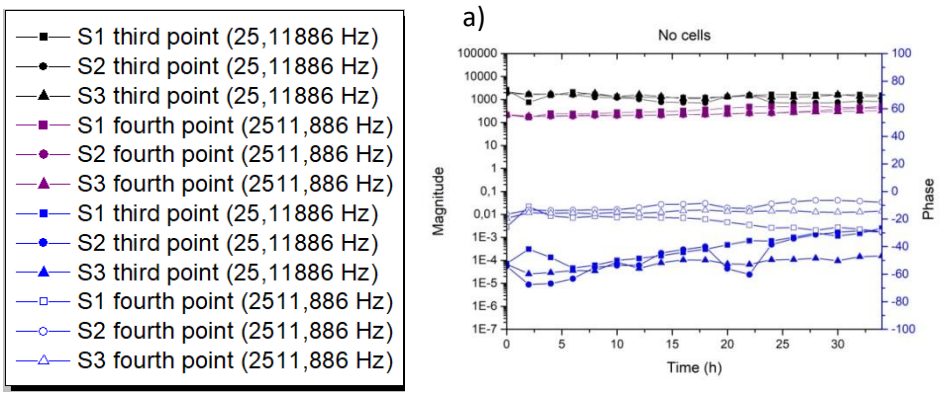

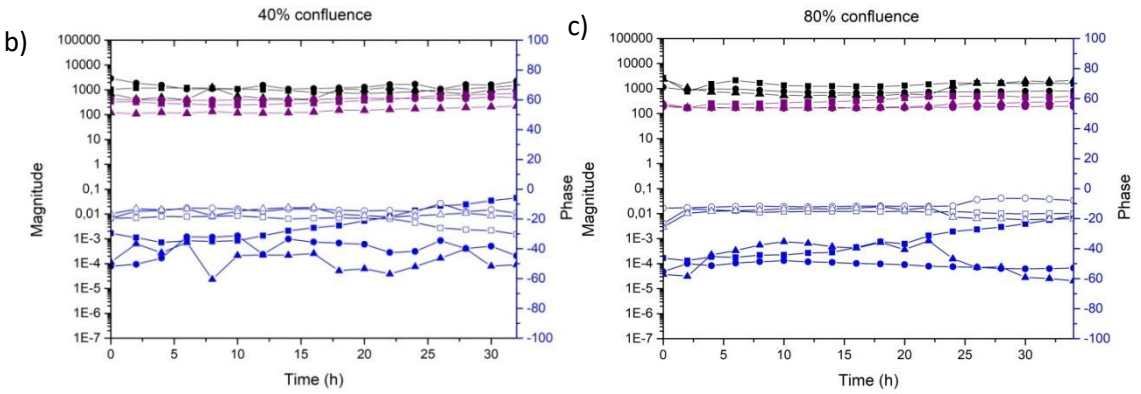

Figure 30. Study of consistency of points 3 and 4 (both above the cut-off frequency) in the three setups in conditions a) without cells b) 40% of confluence and c) 80% of confluence. At high frequencies, the magnitudes are not as affected by the noise when compared to the low frequencies. In the same way as before, the magnitude variation is around one order of magnitude, whereas phase variation is around 60 degrees.

5.2.3 Polar plots: tendency between 0h, 24h and 36h

In the first place, the Nyquist plots were obtained in order to identify a general and consistent tendency in our IDEs. It can be appreciated from the three figures (31, 32 and 33) how the arc described by the setups is not a perfect circle but a depressed one. This justifies the use of the constant phase element in our electrical equivalent circuits.

Moreover, there is a general tendency in the three different conditions tested, which are without cells, 40% of confluence and 80% of confluence. In all these three cases the Nyquist arcs tend to decrease with time with respect to their initial measurement at t = 0 h.

Setup 1 is the one that best matches with the theoretically predicted behavior of the IDE. In the absence of cells, all the arcs start at the same point impedance. This starting point is associated with the solution resistance of the electrical equivalent circuits, thus it is expected to remain constant over time unless another variant is introduced in the system, such as cellular presence.

In all the three setups, the 40% and 80% confluence arcs seem more distorted than their respective control without cells. However, this observation is too unspecific to draw a further conclusion (see the discussion at point 6.2 for more information). The initial depressions before the semicircles are associated with inductive behaviors due to the absence of passivation of the electrodes.

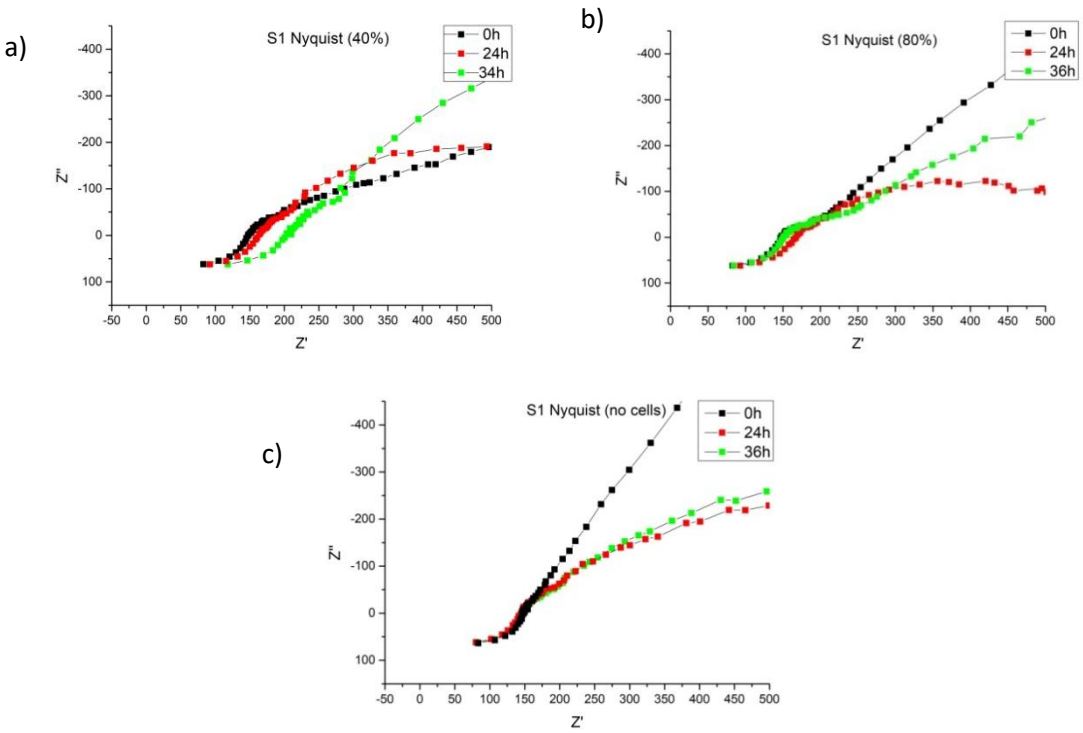

Figure 31. Nyquist plots of setup 1 in the three conditions a) without cells b) 40% of confluence and c) 80% of confluence. Starting point of the diagram is associated with the resistance of the solution. The semi-arc described by the curves is associated with the non ideal behavior of the capacitor, justifying the use of the CPE.

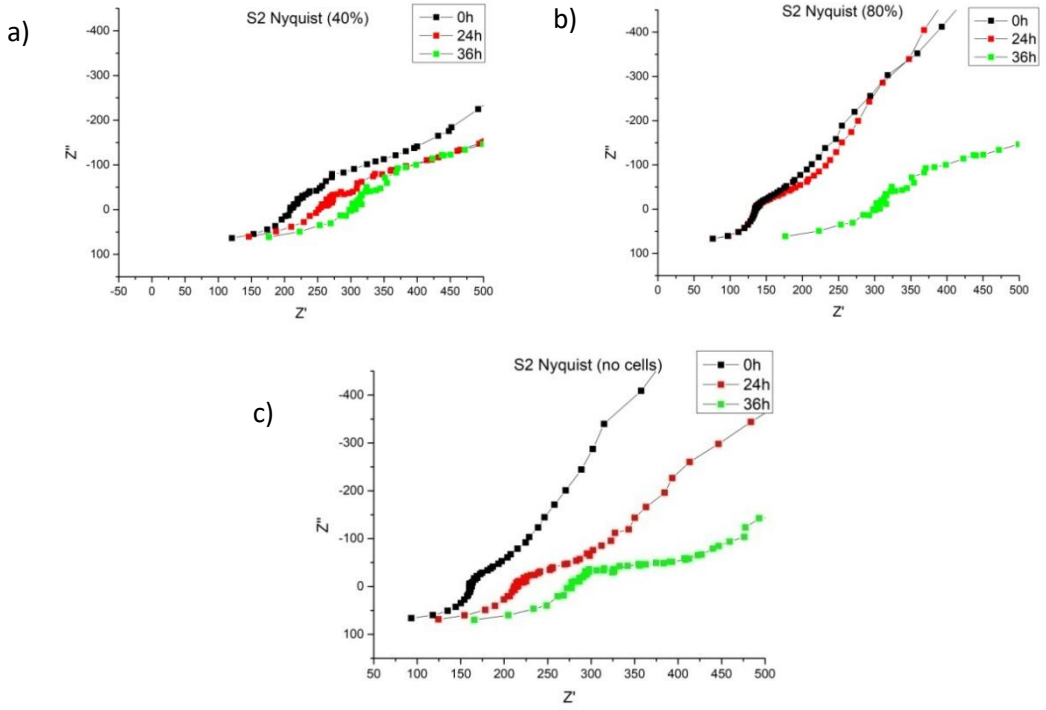

Figure 32. Nyquist plots of setup 2 in the three conditions a) without cells b) 40% of confluence and c) 80% of confluence. Starting point of the diagram is associated with the resistance of the solution. The semi-arc described by the curves is associated with the non ideal behavior of the capacitor, justifying the use of the CPE.

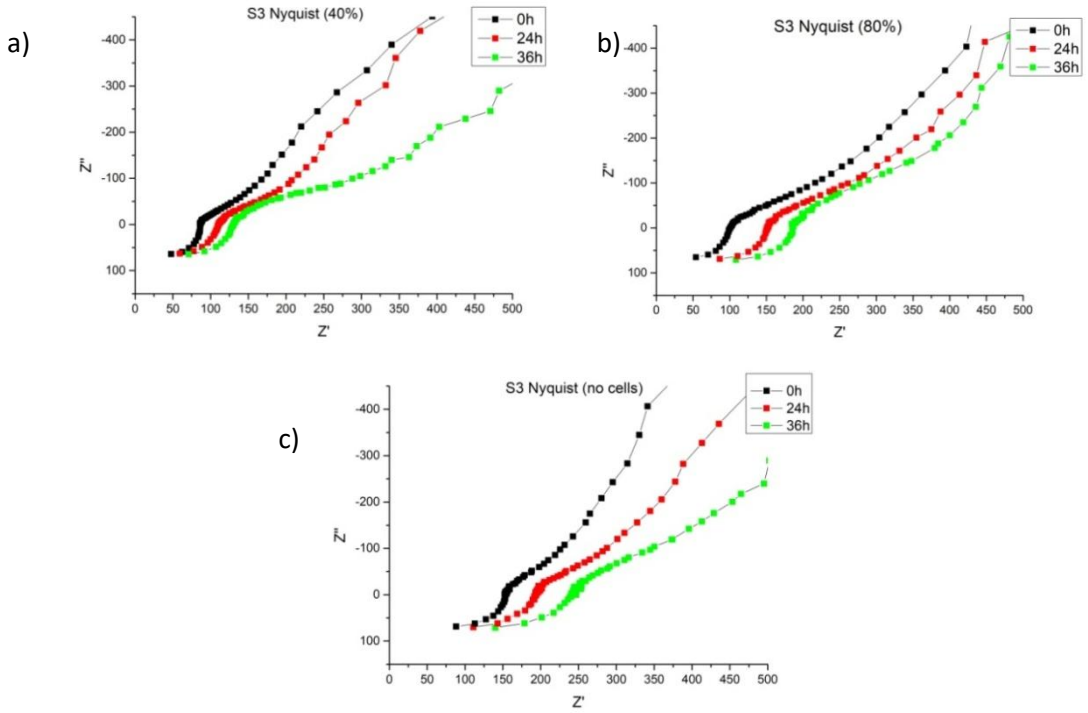

Figure 33.Nyquist plots of setup 3 in the three conditions a) without cells b) 40% of confluence and c) 80% of confluence. Starting point of the diagram is associated with the resistance of the solution. The semi-arc described by the curves is associated with the non ideal behavior of the capacitor, justifying the use of the CPE.

5.2.4 Equivalent electrical circuit fitting examples: pre-attachment and attachment in both circuits

Two equivalent circuits were proposed to characterize the cellular phenomena in terms of impedimetric changes. In both of them, the cellular presence is understood in terms of the addition of another time constant element, that is, a constant phase element (CPE-cell) in parallel with a resistor (R_{gap}). The difference between both relies in the fact that in circuit 1, this new time constant element is placed in parallel with the polarized resistance (R_P), whereas in circuit 2 it is placed in series with both the constant phase element (CPE) and the polarized resistance (R_P).

In the following fitting examples, shown in figures from 34 to 36, it can be seen how the response of the circuit changes in both magnitude with respect to time under the cellular presence. This change in the magnitude curves is understood from the electrical perspective as the addition of another time constant (a resistor in parallel with a capacitor) due to the cellular presence, as it was theoretically predicted. Phase became also different with respect to the controls with time. However, as it has been shown that

the phase became very affected by the noise at low frequencies, a better implementation is needed to extract further information from it.

These graphical representations were analyzed in parallel to the SEM images of the cellular culture on the sensor at different times. The visualization, which is detailed in next section (see 5.3 for further information) served as a confirmation that the electrical change detected corresponded to a real and relevant cellular phenomenon, which was cellular attachment.

The change detected in the magnitude started at t = 12 h, which has been stated as the starting attachment hour. This qualitative change is shown in the following figures, in which pre-attachment corresponds to times smaller than 12 h and attachment corresponds to times bigger or equal 12 h.

Pre-attachment:

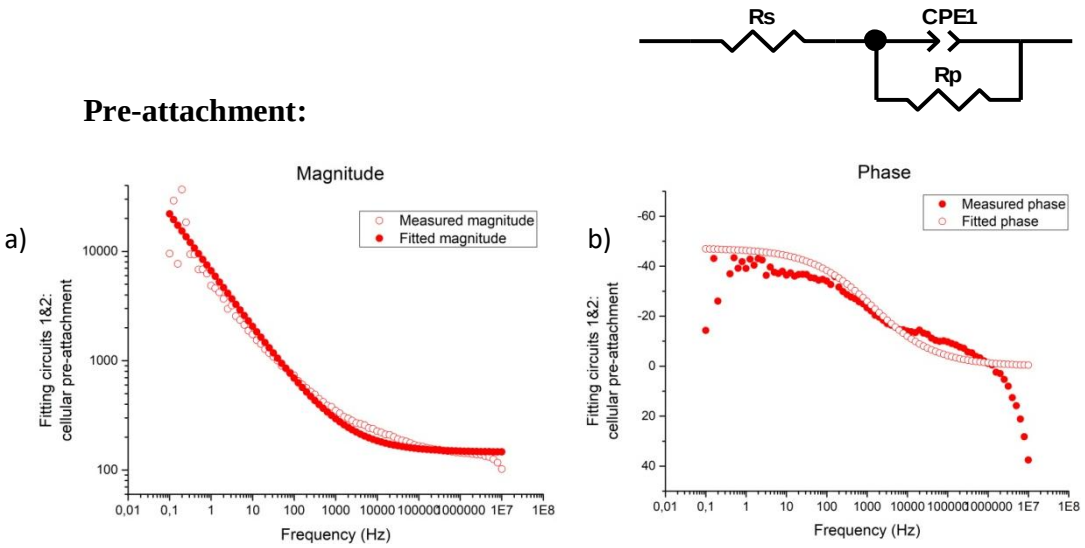

Figure 34. Pre-attachment equivalent circuit fitting of setup 1 at t = 4 h and 40% of confluence in both a) magnitude and b) phase. Red dots correspond with the measured empirical data, whereas white points correspond with the theoretical values employed to fit this data with a theoretical equivalent circuit. In both cases, the magnitude is better fitted than the phase. Noise reduction to guarantee a better fit is the next step.

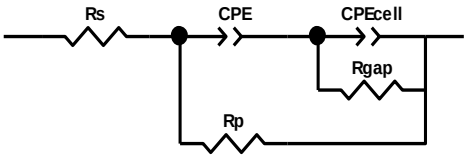

Attachment: Equivalent circuit 1:

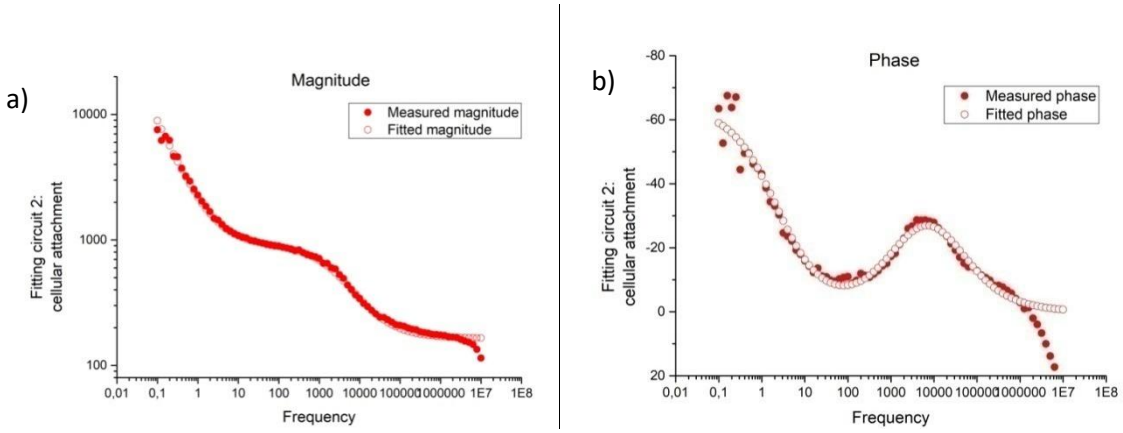

Figure 35. Attachment equivalent circuit 1 fitting of setup 1 at t = 26 h and 40% of confluence in both a) magnitude and b) phase. Red dots correspond with the measured empirical data, whereas white points correspond with the theoretical values employed to fit this data with a theoretical equivalent circuit. If these graphs are compared with figure 32, it is clearly appreciated that the response has changed: another constant element has appeared. The magnitude is better fitted than the phase. Noise reduction to guarantee a better fit is the next step.

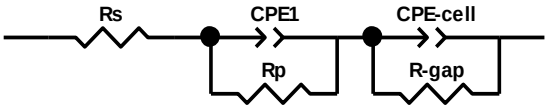

➢ **Attachment: Equivalent circuit 2:**

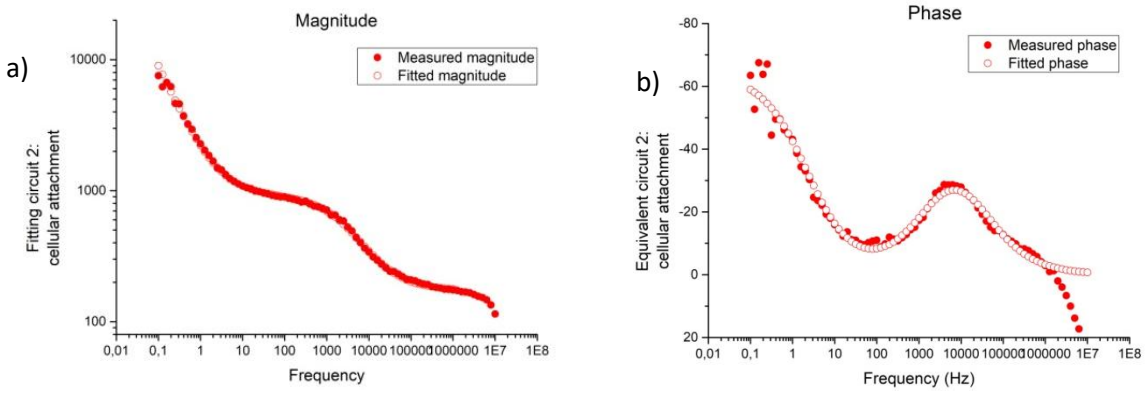

Figure 36. Attachment equivalent circuit 2 fitting of setup 1 at t = 26h and 40% of confluence in both a) magnitude and b) phase. Red dots correspond with the measured empirical data, whereas white points correspond with the theoretical values employed to fit this data with a theoretical equivalent circuit. If these graphs are compared with figure 32, it is clearly appreciated that the response has changed: another constant element has appeared. The magnitude is best fitted than the phase. Noise reduction to guarantee a better fit is the next step.

➢ **Comparative between fitting errors percentages: setup 1 at t= 26h 40% of confluence:**

Graphically, differences between both equivalent electrical circuits are hardly distinguishable. Table 4 shows the numerical fitting errors percentages in the example fitting case of setup 1, at confluence of 40% and times t = 2 h and t = 26 h, bearing in mind that t = 26 h was proven to hold the cellular attachment on the sensor (see 5.3 to check the SEM images).

From this table, it can be clearly appreciated how in the case of circuit 2, the errors are smaller when compared with circuit 1. This comparison was repeated several times, with similar results as the one shown. Next section compares the CPE variation standard errors for all the attachment hours, confirming that fitting with circuit 2 ensures less error and therefore less variability.

Table 4. Comparison of the percentage errors of a given setup (setup 1) at two different times (t=4h and t=26h) for the same condition (40% of confluence). Orange cells correspond to errors much higher than expected. CPE-T cell is a reliable parameter that can be used to discard one circuit. The percentage error of this circuit element decreases with the second circuit by 10%.

	Rs	CPE-T	CPE-P	CPE-T CEL	CPE-P CELL	Rgap
Pre-attachment	157,7	5,72E-05	0,53	-	-	-
Error (%)	4,715	5,2596	2,03	-	-	-
Attachment circuit 1	164,4	1,64E-04	0,71	2,22E-06	0,68	741,7
Error (%)	2,22	2,93	0,01	25,82	3,55	3,49
Attachment circuit 2	172,2	1,63E-04	0,71	2,07E-06	0,69	740,3
Error (%)	1,75	1,90	1,18	15,76	2,21	2,06

The polarized resistance of both of the attachment circuits (circuit 1 and 2) increases with respect to time, achieving a magnitude more than ten times bigger than the initial control measurements. The electrical implication of such a big value is that

the current will flow just through the constant phase element of the circuit instead taking the path between the electrodes. Therefore, its role in the equivalent circuit is negligible and that is the reason why instead of being presented in the table it is commented.

5.2.5 Monitoring circuit elements in cellular pre-attachment

As anticipated before, the time that has been identified as the moment in which the cellular attachment takes place on the IDE corresponded to t = 22 h. This change in the impedance response of the circuit was compared with the images from the SEM visualization (see next point, 5.3, for further information), confirming that the electrical change detected was due to the cellular attachment.

During the first 20 hours, therefore, the phenomenon observed is just the ionic conduction of the biological medium. Changes in the double-layer capacitance are thus produced by changes in ion concentration. Figure 37 represents such differences, normalizing the values with respect the CPE values of time t = 0 h, whereas table 5 contains the standard errors of this variations, which are high.

It can be appreciated how there is not a clear tendency in the overall ionic interchange; however, it is clear from the equivalent circuit fittings (see previous point) and confirmed by posterior SEM images (see 5.3) that the cellular attachment has not taken place yet, and therefore this ionic study is out from the scope of this work.

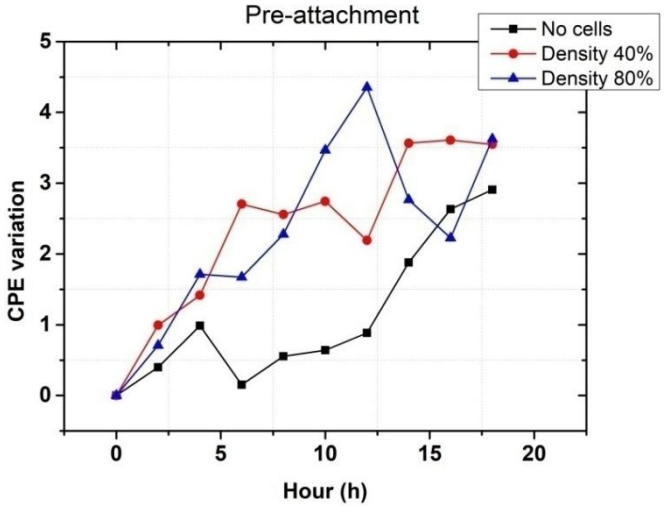

Figure 37. CPE variation during the first 20 h. There is not a clear tendency in this graph, nor any significant difference between the three different conditions. As attachment has not taken place yet, this growing tendency is believed to be produced by the ionic interchange and thus provides no relevant information to this Bachelor Thesis.

Table 5. Standard errors of the first 20 h for the three conditions. All the included standard errors are higher than acceptable. These huge errors remark the necessity of reducing the noise source trying this way to reduce variability.

Time (h)	Standard error NC	Standard error 40%	Standard error 80%
0	0	0	0
2	0,24	0,60	0,14
4	0,60	0,63	0,93
6	0,02	0,27	0,92
8	0,05	0,96	1,57
10	0,39	1,29	2,54
12	0,51	1,61	3,51
14	1,08	2,11	1,63
16	1,68	1,98	1,04
18	1,80	2,07	1,93
20	0,45	2,24	1,39

5.2.6 Monitoring circuit elements in cellular attachment

From the empirical data obtained, we hypothesize that cellular attachment influence was not noticed until the hours from 22 on, when the magnitude changed in the empirical data of cellular confluences 40% and 80%. This electrical change modified the electrical equivalent circuit by adding another time constant element. Once we were sure that this change was presented in all the setups for the cellular conditions, next step was to monitor the change of the equivalent circuit elements over time in order to find a general tendency.

Values represented in figures 38 and 39 are normalized with respect the time = 22h, when the cellular attachment has been identified. From these images, it can be clearly distinguished that there exists a tendency in the variation of the double layer capacitance with respect the control. This overall tendency coincides with the one observed in the Nyquist's plots; it can be observed how the variation when cells are added to the medium results in a decrease of the curve with respect the control (sensor without cells). Regarding the solution resistance, as the volume of the cellular culture

medium remains the same during the whole process, its monitoring is not presented here as a result providing further information.

Furthermore, regarding the two different confluences, it can be appreciated how the 40% of confluence is generally above the 80% one. This can lead to conclude that the cellular presence results in a decrease of the double layer capacitance of the circuit. However, tables 6 and 7 show that errors are bigger than acceptable, and thus differences between confluences are not as well defined as expected.

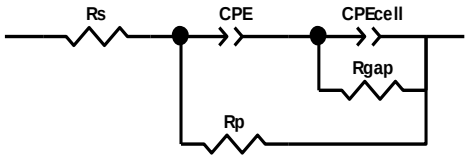

5.2.6.1 Electrical circuit 1

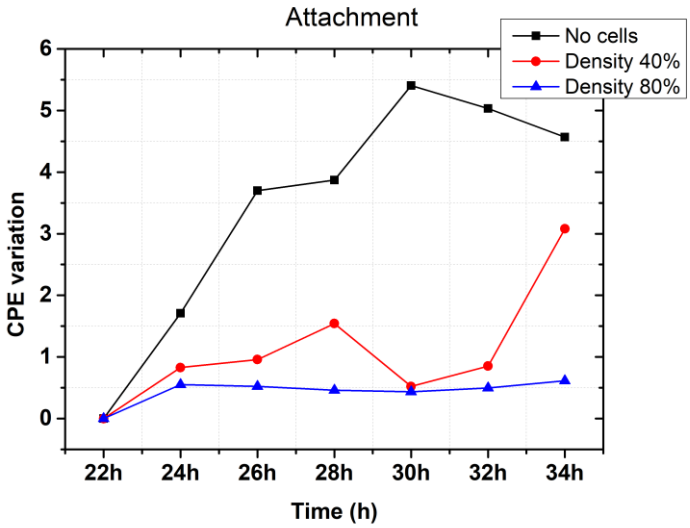

Figure 38. CPE variation from 22 h on using equivalent circuit 1. Attachment has been produced. This cellular phenomenon results in a decrease of the CPE that is inversely proportional to the area covered by the cells.

Table 6. Standard errors from 22 on, for the three conditions using equivalent circuit1. Most of the included standard errors are higher than acceptable. These huge errors remark the necessity of reducing the noise source trying this way to reduce variability.

Time (h)	Standard error NC	Standard error 40%	Standard error 80%
22	0	0	0
24	1,60	0,73	0,18
26	3,31	0,65	0,14
28	3,60	1,04	0,18
30	5,15	0,18	0,24
32	4,61	0,29	0,23
34	3,87	2,29	0,14

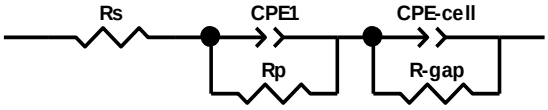

5.2.6.2 Electrical circuit 2

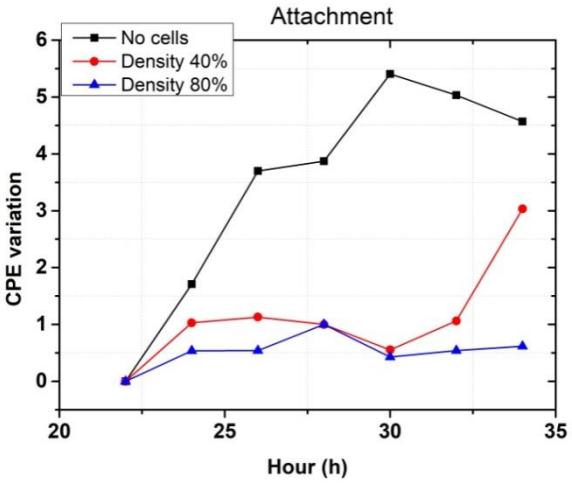

Figure 39. CPE variation from 22 h on using equivalent circuit 2. Attachment has been produced. This cellular phenomenon results in a decrease of the CPE that is inversely proportional to the area covered by the cells.

Table 7. Standard errors from 22 on, for the three conditions using equivalent circuit 2. Most of the included standard errors are higher than acceptable. These huge errors remark the necessity of reducing the noise source trying this way to reduce variability.

Time (h)	Standard error NC	Standard error 40%	Standard error 80%
22	0	0	0
24	1,60	0,63	0,17
26	3,31	0,54	0,16
28	3,60	4,23E-05	2,53E-05
30	5,15	0,14	0,24
32	4,61	0,21	0,19
34	3,87	2,31	0,14

5.2.6.3 Comparative between standard errors of circuits 1 and 2

Table 8 compares the standard errors and deviations of both electrical circuits. According to this table, circuit 2 presents lower standard errors than circuit one, especially in the 40% of confluence condition, being better in terms of the fitting with the empirical values.

Table 8. Comparison between the standard errors of circuits 1 and 2. Orange cells correspond with a standard deviation bigger than 0.05.According to this table, circuit 2 presents lower standard errors than circuit one, especially in the 40% of confluence condition.

Time (h)	S.E 40% circuit 1	S.E 40% circuit 2	S.D 40%	S.E 80% circuit 1	S.E 80% circuit 2	S.D 80%
22	0	0	0	0	0	0
24	0,73	0,63	0,07	0,18	0,17	0,01
26	0,65	0,54	0,08	0,14	0,164	0,01
28	1,04	0,00	0,73	0,18	0,00	0,13
30	0,18	0,14	0,03	0,24	0,24	0,00
32	0,29	0,21	0,06	0,23	0,19	0,02
34	2,29	2,31	0,01	0,14	0,14	0,00

5.3 Cell visualization

5.3.1 Inverted microscope images

During the cell-substrate impedance spectroscopy some measurements scontrol pictures of the cells on the IDE were taken to asses that the electrical field did not produce a massive cellular death or apoptosis.

Table 9 shows the evolution of one area over time in the cell-substrate impedance spectroscopy experiment of setup 3. It can be appreciated that at t = 36 h the cells have been spread over the sensor, becoming less rounded and bright.

Table 9. Images during spectroscopy experiment. Inverted microscope.

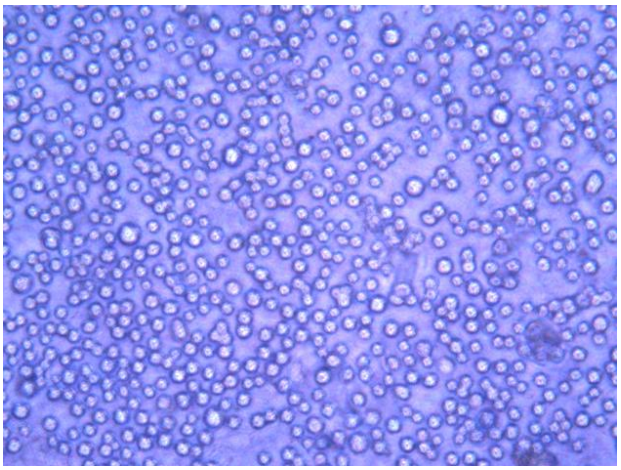	**Setup 3, 0h:** HaCaT at 80% of confluence were seeded over the sensor and the electric field was induced to perform the cell-substrate impedance spectroscopy experiments.
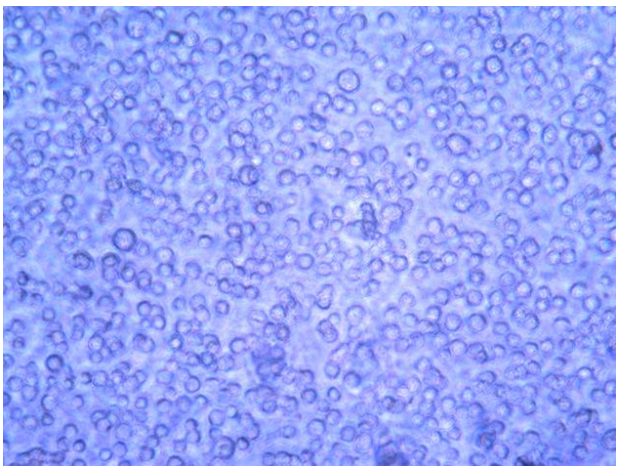	**Setup 3, 36 h:** After 36 h, cells have attached to the IDE, becoming less bright and proliferating. Induced electrical field did not produce cell apoptosis.

Furthermore, in order to check whether the cells were attached on the electrode fingers or not, another image was taken using a bigger magnification. Figure 40 clearly shows the electrode in the middle of the image. Unfortunately, due to the electric field

that the sensor was generating while the images were taken, bubbles distorted the actual image and cellular attachment on the sensor was not ensured.

Figure 40 was insufficient to guarantee this attachment; it is shown here because it served us as justification to visualize the cellular morphology using the scanning electrode microscope (SEM).

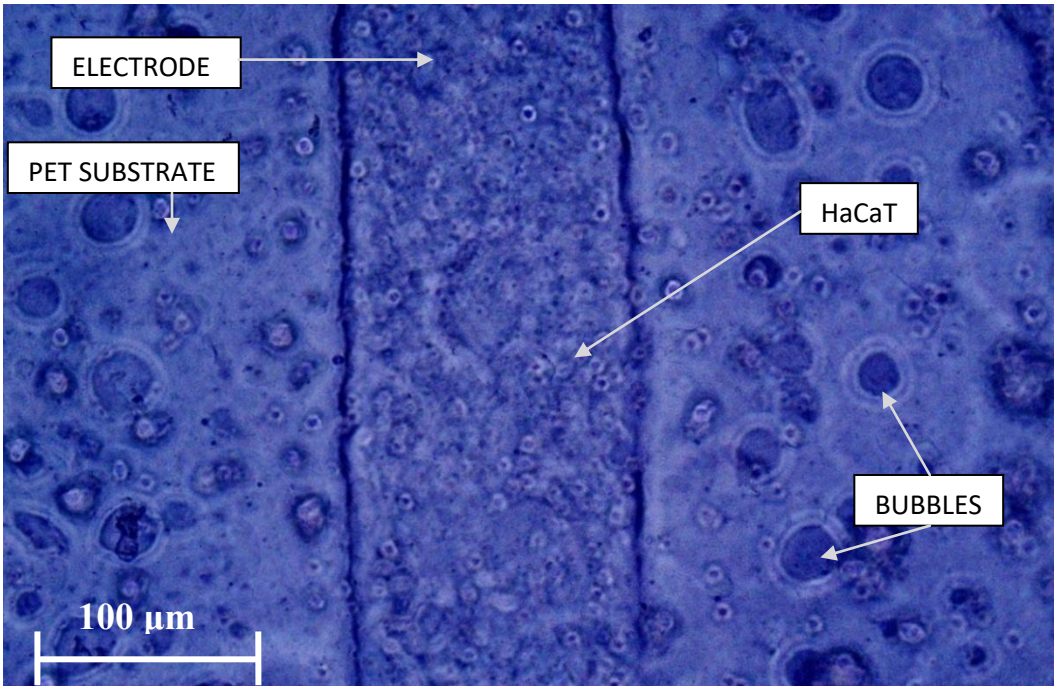

Figure 40 Cells on the electrode. Although some HaCaT cells could be distinguished, air bubbles produced due to the induction of the electrical field distort the image. This image is presented here because it served us as a justification to visualize our samples at the SEM microscope.

5.3.2 SEM images

- Cell control: cells on the plate (without sensor), 12h

Figure 41 shows the HaCaT cells on the plate of the Petri dish. It can be appreciated how these three cells have been already attached on the plate, as they are flattened over the substrate becoming less bright.

This image served as a control measurement. As the same protocol was done for all the samples, having this control served us to check that the fixing was performed correctly. Furthermore, some white dots can be appreciated over the cells. These dots, which are found in all the images obtained with the SEM involving cellular cultures,

have been identified as crystals formed during the fixing procedure of the samples and have no relevant biological meaning.

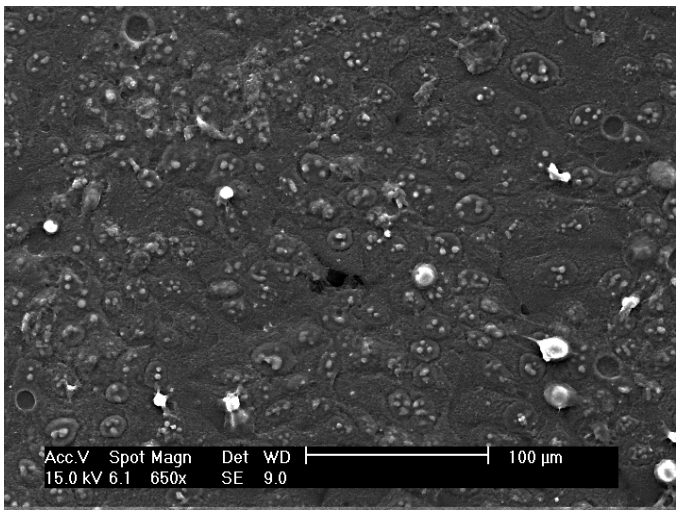

Figure 41 Cells attached on the Petri dish. Cells are flattened over the surface, as their shape has became flattened instead of rounded. This image served us as a control to ensure that the fixing was made correctly.

- Sensor control: sensor without cells

Figure 42 represents one of the electrode bands of the same metallic ink of the IDE on PET substrate. As the available amount sensors were limited, the image was obtained using some of the samples provided by the Fraunhofer institute, in which the metallic ink electrodes had 500 µm of width.

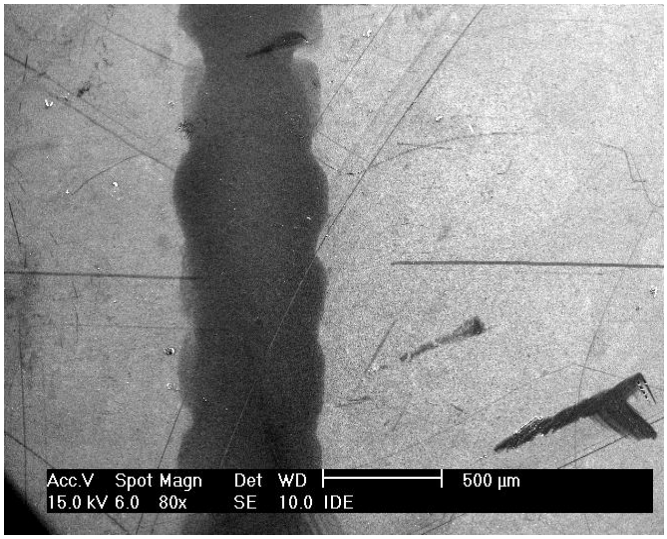

Figure 42. IDE's electrode (dark band) on PET substrate (bright background).

- Comparison between hours: 12 h, 18 h, 22 h and 40 h

Table 10. Detailed comparison between hours 12 h, 18 h, 22 h and 40 h

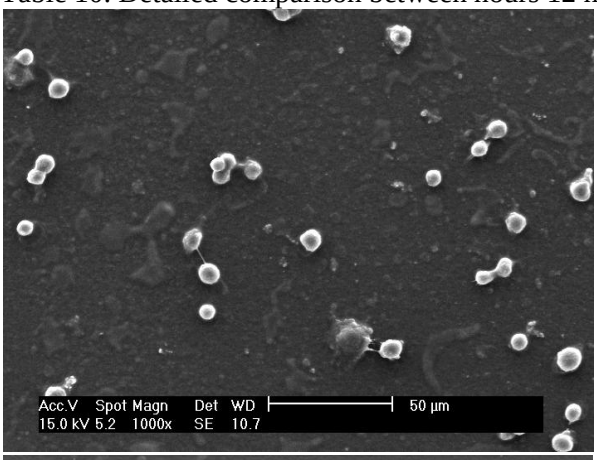

12 h: although the cells are in contact with the sensor, the attachment has not been produced yet. Unlike figure 38, in which the cells have been already attached on the plate, cells present a rounded and bright morphology.

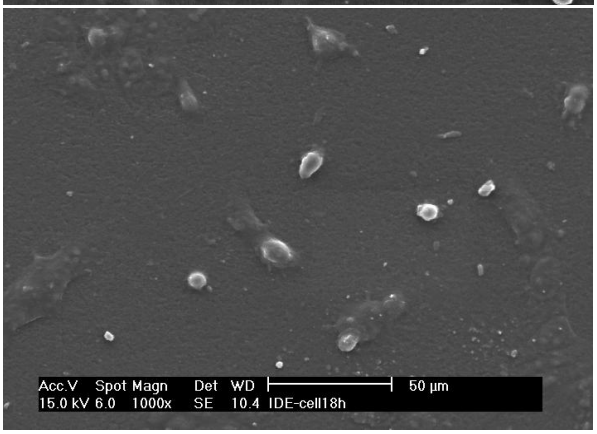

18 h: cells have started attaching in some areas, becoming more flattened and less bright when they are in contact with the IDE. However, overall attachment has not been produced in the whole IDE's surface,

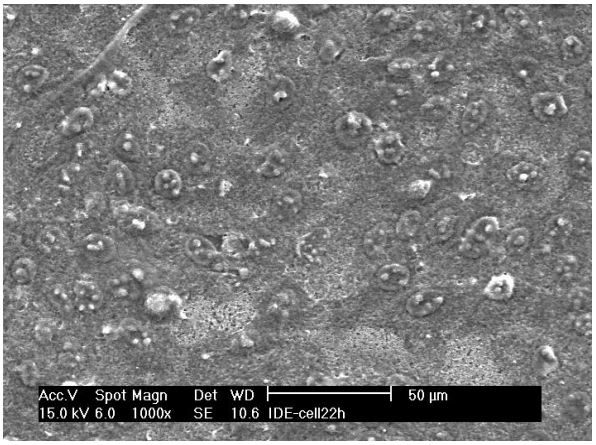

22 h: this has been identified as the critical hour in which attachment has been already produced. It can be appreciated how the majority of the cells have been attached and started proliferating, showing a morphology similar to the control (figure 38).

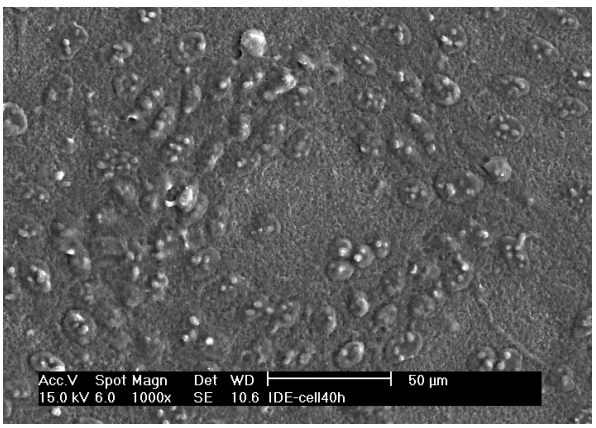

40 h: in the hours that followed t = 22h, the cells have attached completely to the IDE, as it was expected by the cellular viability test, the IDE supports cell viability allowing the cellular culture to spread over the sensor.

Table 10 presents a comparison of how the cellular culture behaves over time in contact with the sensor. From it, it can be clearly appreciated how at t = 18 h some cells had started the attachment in some areas, but this attachment was still partial and not extended, as the majority of the cells remained rounded and bright. At t = 22 h the HaCaT culture had attached globally on the IDE, proliferating on it.

From 22 h on, therefore, the change detected on the impedance response of the empirical data can be associated with a real and relevant biological phenomenon: the cellular attachment. SEM images served then as a confirmation of the relevance of the change in the impedance response detected by the IDE, in which the electrical equivalent circuit became best fitted with the circuits proposed for the cellular phenomenon.

- Marker bands: hour 40

From the images of the previous table, it can be appreciated how the images have lost the contrast required to distinguish the electrode from the PET substrate when the cells were seeded over the sensor.

In order to ensure that the cells were attached not only to the PET but also to the electrodes, borders of the electrodes were marked using samples of ink + PET of 500 μm of width.

Figure 43 shows how effectively the cultured HaCaT cells are attached to all the IDE regions including the electrodes in a homogeneous way.

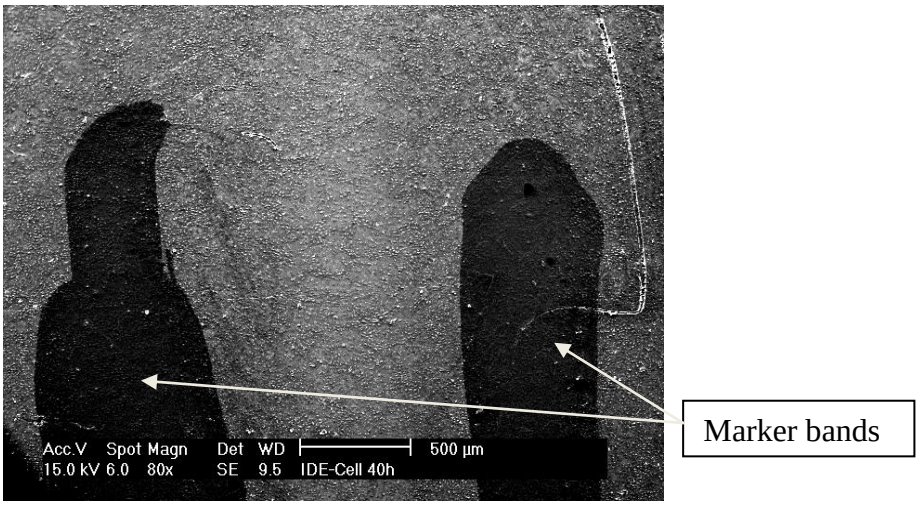

Figure 43. Cells attached on the sensor, where marker bands represent a finger electrode.

5.4 Solution design: model 2 and model 3

Figure 44 shows the obtained results. The first experiment result shows how the noise reduction is achieved from the first moment. It has shown that the lack of a proper welding and passivation results in an increase of the impedance modulus when compared with the new implementation.

Finally, the second experiment shows that the passivation of the IDE results in a small increase of the impedance modulus, that is corrected at high frequencies, as both magnitude measurements converged from 100 Hz on. Overall, this last implementation seems to be a step forward for the continuation of this project.

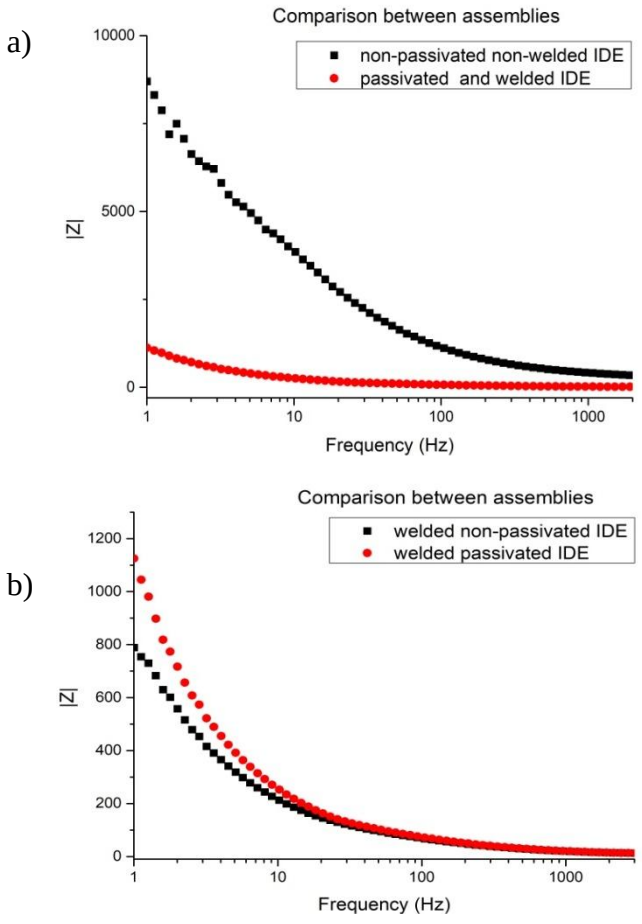

Figure 44. Impedance magnitude of model 2, both with the new and the old implementations. Firstly, in a) the new implementation was compared with the old one, showing the reduction of noise at low frequencies. In b) the same IDE was measured in magnitude before and after the passivation, showing a displacement in the starting impedance modulus without no other variation. This first measurements served as proof of concept of the improvement achieved.

6. Discussion of the results and general conclusions for the solution design

6.1 Characterization of the sensor without cells

The implementation without PDMS ring was chosen to continue with the experiments, as we hypothesize that the curing process of the PDMs over the IDE probably affected its performance, compromising its phase and magnitude.

In addition, 20 mV was selected as the applied voltage potential to work with. Between the 5mV and the 20 mV of voltage, this potential is less sensitive to noise at low frequencies and it is still a safe tension value to apply to the HaCaT without inducing cell apoptosis, as their resting potential is higher to the value induced [34].

The bioreactor's assembly showed the expected decrease in variability that was necessary to work with cells in a consistent way. It has remarked thus the necessity of using the bioreactor not only when dealing with cellular cultures, but also with the controls. Furthermore, solution resistance, R_s, has been successfully associated to the volume of the solution, having this parameter identified for the following interpretations.

Once the IDE implementation was fixed, the control measurements started. The fitting of the control measurements (without cells) with our proposed equivalent circuit reported god results, as the impedance response remained constant over time for the three setups.

Concerning the picoamperimeter measurements, after observing the inconsistency problematic and performing a control AC impedance measurement, the conclusion extracted was that the IDE's lifetime was limited. This result served to make us realize that reusing the IDE could induce some deterioration of the sensor that can compromise its performance. In order to characterize and this deterioration, next experiments with the new sensors must start with a conductivity study that compares the sensor conductivity before and after obtaining the measurements with the impedance/phase analyzer.

6.2 Spectroscopy of cell-substrate impedance.

Regarding the cell viability assay, since p-value obtained in all the cases was bigger than 0,05, both the PET itself and the PET with the metallic ink supported cell viability in the same way as a Petri dish. The proliferation graph indicated that, the three times that this experiment took place, there was an increase in the cellular metabolic activity with respect day 1, which means that in the three conditions the cells were not only behaving as the control, but proliferating over the IDE as expected.

The study of stability has remarked that the right pathway was being followed. However, it also remarked that noise affected low frequencies points in the range from 0,1 Hz to 10 Hz, inducing variability in the measurements.

Polar plots show the general tendency of the modulus of the overall impedance to decrease with respect to the control. However, the three setups differ too much from each other to draw further conclusions from the graphs. In the three conditions it can be clearly appreciated how the arcs are not perfect semicircles but depressed ones, which confirms that in this work we are not dealing with perfect capacitors and constant phase elements are needed in order to properly build the electrical equivalent circuits.

Concerning the electrical equivalent circuit fitting, it can be concluded that the presented fitting with the empirical data is coherent with the theoretical perception of the change induced by the cellular presence. In the case of the controls, the impedance response remained unchanged over time. In the case of the measurements performed with cells, the impedance response changed over time, being t = 22 h the time from which the magnitude of the impedance started changing. From this time on, the electrical equivalent circuit changed in order to adjust to the empirical data. This change was understood as the addition of another time constant element into the circuit.

Once this electrical change was detected, next step consisted of monitoring the different electrical elements of the two equivalent circuits proposed in order to find a general tendency. This tendency was identified in the case of the constant phase element representing the double-layer capacitive of the sensor (CPE) from t = 22 h on.

The CPE variation changes observed from 0 h to 22 h corresponded to the ionic interchange of the medium in the case of the control, and of the medium and the cells floating on it in the case of the 40% and 80% of confluences. The pre-attachment

phenomena graphs presented a chaotic movement of CPE values, as the ionic interchange is not a stable and constant phenomenon.

From the 22 h to the 36 h that followed, the cellular culture had reached the electrodes and attachment had started taking an important role, reflected both in the change of the circuit and in the values obtained of CPE. There was a relevant tendency of the constant phase element to decrease with respect the control under the cellular presence, decreasing in a way inversely proportional to the area covered by the cells.

Concerning the different equivalent circuits proposed for the attachment process, differences in the standard errors are only significant in a few cases, in which circuit 2 presented a lower standard error with respect circuit 1. It is for this reason, together with the comparative of fitting errors, that circuit 2 was considered the most suitable circuit for describing the cellular attachment phenomena. This indicates, from an electrical perspective, that the current was always following the same path towards the dielectric layer and the cells attached on the electrode's surface.

The images obtained with the inverted microscope with phase contrast served us to visualize that HaCaT epithelial cells were attached and proliferating on the IDE during the experiments. This proves that the induced electrical field did not induce cellular apoptosis and still served us to detect cellular changes and associate these changes with cellular attachment. Due to the presence of some air bubbles, the samples were taken to the scanning electrode microscope to assess the time in which cells attached to the IDE.

From the images obtained with the SEM microscope, the cellular attachment process had been identified to start playing a predominant role approximately around t = 22 h. This qualitative information coincides exactly with our equivalent circuit change. In that way, it has been proven that the IDE has obtained the same information than the SEM, but in real time and without the necessity of fixing the cells and thus without the multiple repetitions that introduce possible variations.

6.3 General conclusions for the solution design

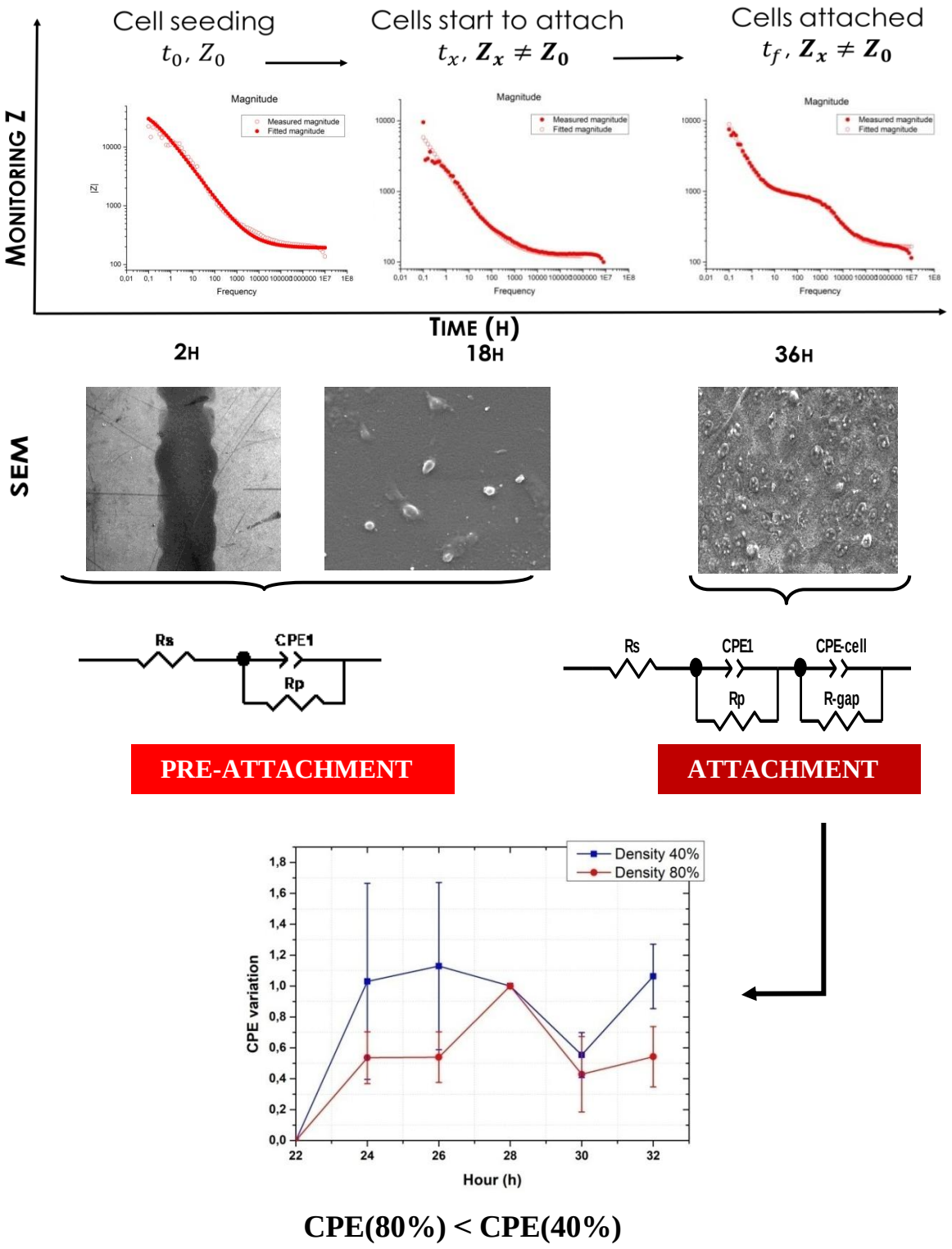

Figure 45. Schematic representation of the general conclusions of this project. Summing up, this Bachelor Thesis has been able to characterize a given IDE applied to cellular culture. In this work, it has been proven that this kind of sensors can be used to detect cellular attachment in real time, with the same accuracy than a visual detection by means of the SEM, but with the advantage of avoiding the fixing of the cells and thus their death and the repetition of visualization. Noise is the main drawback of the method proposed here.

All in all, this first approach in the characterization of the IDE (model 1) applied to cellular cultures has resulted in a series of conclusions that were crucial for the proposed solution design and will thus influence the following work.

In the first place, it has served to link different circuit elements to the real measured data. The electrical equivalent circuit selected has proven its efficiency as a suitable model by which biologically relevant information can be obtained. My work has proved that these sensors can be used to detect cellular attachment *in vitro* in real time, with the accuracy that other imaging techniques such as SEM can provide, but keeping the simplicity in the measurement and the cellular culture alive.

By looking at the obtained data, a future implementation of the sensor as an indicator of cellular activity in severe burn patients seems quite possible. It has proven to avoid the long-time consuming current procedures of imaging cells (in the burns case scenario via biopsies), at least in terms of cellular attachment detection.

To continue, due to the noise presented especially in the frequency range from 0,1 Hz to 10 Hz, this Bachelor Thesis has exposed the absolutely necessity of isolating the electrodes from the medium via its passivation, as well as to replace the adhesive tape used as contact between the electrode and the cable by a more optimum welding. This has been achieved in model 2 by using a conductor resin and an insulator tape.

Results obtained with model 2 present an improvement in the new implementation in terms of noise, that is expected to be translated into a decrease in variability in the future experiments.

Failing in the DC characterization due to the lost of the sensor behavior has remarked the absolute necessity of stop reusing the setups in the following experiments and performing a control conductivity experiment before and after any impedance spectroscopy experiment.

Finally, as the final aim of this project is directed towards a 3D *in vitro* implantation mimicking a human tissue, it has been noticed that semiconductor metal inks are not the best option in terms of the biocompatibility. The model 1 sensor in a tissue can trigger the host response due to the metal ions liberation; this is the rationale behind the idea of characterizing a sensor with a polymeric ink, proposed in the following point by model 3.

7. Further studies

This work has pursued a whole understanding of the impedance spectroscopy principle applied to interdigitated sensors. A novel design based on previous results has been proposed, reporting promising results in terms of noise reduction that will allow the detection of relevant cellular phenomenon.

So far, the IDE has faced the challenges related with *in vitro* assays and the correlation of the equivalent circuit parameters with the real and relevant cellular phenomena in a 2D cell culture environment. To continue with this 2D *in vitro* approach, models 2 and 3 should be tested, in terms of both impedance spectroscopy and continuity. With these new measurements, variability and deterioration of the sensors will be assessed and controlled.

As this work has been performed always bearing in mind the implantation of the IDE in tissue, next steps must be done forward the implantation of the IDE into a 3D culture *in vitro*, which will contain both the epidermal and the dermal layers of the skin organization. In this scenario, sacrificial substrates allowing the transpiration of the tissue through the spacing of the IDE must be considered. Sacrificial substrates will allow the printing of the IDE over a substrate and the posterior elimination of this substrate once the sensor is introduced in the living tissue.

Nowadays, wearable epidermal devices printed on sacrificial flexible substrates are being tested and proposed to the personalized medicine field reporting good results in terms of cost-effectiveness and signal recording [38]. Figure 46 includes a schematic representation of the process of attaching the wearable sensor on the skin (epidermis) of the patient. In this case, a water soluble tape is employed as the sacrificial substrate of the sensor, made of copper.

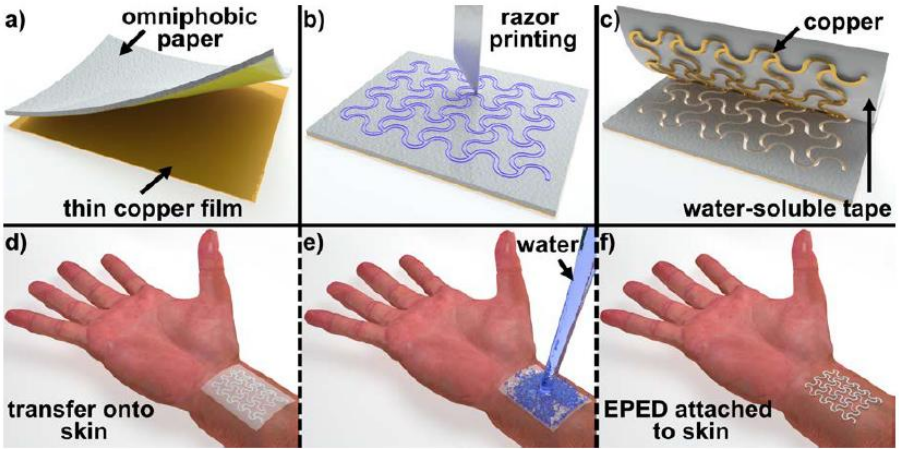

Figure 46. Schematic representation of the process of attaching the wearable sensor on the skin (epidermis) of the patient. After transferring the pattern onto the water soluble tape, the sensor is glued to the skin of the patient by means of a medical glue. Then, upon the addition of water, the substrate became dissolved and the final wearable flexible sensor remain attached on the dermis of the patient [38].

My proposal consists of bringing this wearable sensors one step further by introducing them at the intraepidermal level. By using polymeric inks instead of metallic ones (model 3), the host response of the tissue will be minimized. The omniphobic cellulose fibers of previous wearable sensors would be suitable for this proposed intraepidermal implantation of the sensor, as the cellulose is moderately biocompatible and can be fully converted to a biocompatible material by means of chemical and/or physical treatment [39].

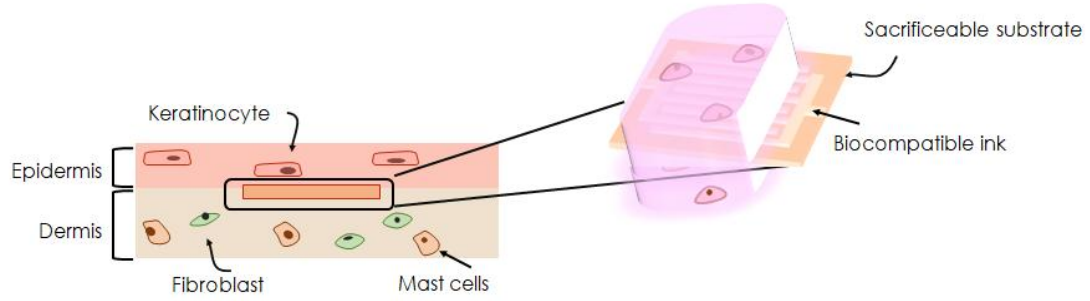

Figure 47. Schematic representation of the sensor embedded in a 3D cellular culture. The future IDE proposed would be printed onto a sacrificial substrate such as omniphobic cellulose that will be dissolved upon the addition of water leaving the IDE itself and allowing the tissue transpiration through the spacing of the interdigitated fingers.

Direct functionalization of collagen over the sensor would be an appropriate solution to enhance the cellular attachment, by mimicking the epithelial cell environment and enhancing the disruption of the electric field created by the sensor. Furthermore, wireless detection must be achieved if the biosensor is thought to stay within the host for a long time.

8. References

[1] S. Carraca and K. Iniewski (Ed), “Handbool of Bioelectronics”, ISBN 978-1-107-04083-0, 2015.

[2] J. S. Danielsa, and N. Pourmanda, “Label-Free Impedance Biosensors: Opportunities and Challenges”, *Electroanalysis*. May 2007 [Online] Available: doi: 10.1002/elan.200603855.

[3] S. Bayoudha, A. Othmane, L. Ponsonnet, H. Ben Ouadaa “Electrical detection and characterization of bacterial pre-attachment using electrochemical impedance spectroscopy-based flow chamber” *Colloids and Surfaces A: Physicochemical and Engineering Aspects*, vol. 318, pp 291-300, Apr. 2008 [Online] Available: doi: 10.1016/j.colsurfa.2008.01.005.

[4] S. MacKay, P. Hermansen, D. Wishart and J. Chen “Simulations of Interdigitated Electrode Interactions with Gold Nanoparticles for Impedance-Based Biosensing Applications”, *Sensors*, Sept. 2015. [Online] Available: doi: 10.3390/s150922192.

[5] T.-T. Ngo, A. Bourjilat, J. Claudel, D. Kourtiche and M. Nadi, “Design and Realization of a Planar Interdigital Microsensor for Biological Medium Characterization”, *Next Generation Sensors and Systems*, pp 23-54, July 2015 [Online] Available: doi: 10.3390/chemosensors6030030.

[6] “National Burn Repository 2016. Chicago, IL: 2016”, *American Burn Association*, [Online]. Available: http://ameriburn.org/education/publications/ [Accessed: 28-Mar-2019].

[7] F. N. Williams, D. N. Herndon, H. K. Hawkins, J. O Lee, R. A Cox, G. A. Kulp, C. C. Finnerty, D. L. Chinkes, and M. G. Jeschke, “The leading causes of death after burn injury in a single pediatric burn center”, *Critical Care*, Nov. 2009 [Online] Available: doi: 10.1186/cc8170.

[8] O. Nunez Lopez, J. Cambiaso-Daniel, L. K Branski, W. B. Norbury and D. N. Herndon, “Predicting and managing sepsis in burn patients: current perspectives”, *Therapeutics and Clinical Risk Management*, vol. 13 Aug. 2017 [Online] Available: doi: 10.2147/TCRM.S119938.

[9] Matthew P. Rowan, Leopoldo C. Cancio, Eric A. Elster, David M. Burmeister, Lloyd F. Rose, Shanmugasundaram Natesan, Rodney K. Chan, Robert J. Christy, and Kevin K. Chung, “Burn wound healing and treatment: review and advancements”, *Critical Care,* Jun. 2015. [Online] Avaiable: doi 10.1186/s13054-015-0961-2.

[10] *Epicel.* [Online]. Available: https://www.epicel.com/patients/index.html [Accessed: 20-May-2019].

[11] D. Church, S. Elsayed,O. Reid,B. Winston,and R.Lindsay, “Burn Wound Infections”, *Clinical Microbiology Rev*, vol. 2, pp. 403-434, Apr. 2006 [Online] Avaiable: doi: 10.1128/CMR.19.2.403-434.2006.

[12] M. J. Farrow, I. S. Hunter, and Patricia Connolly, “Developing a Real Time Sensing System to Monitor Bacteria in Wound Dressings”, *Biosensors (Basel)*, vol. 2, 171-188, May 2012. [Online] Avaiable: doi: 10.3390/bios2020171.

[13] I. Giaever, and C. R. Keese, “Use of Electric Fields to Monitor the Dynamical Aspect of Cell Behavior in Tissue Culture”, *IEEE Transactions on Biomedical Engineering*, vol. BME-33, pp. 242-247, Feb. 1986

[14] C. Lo, C. R. Keese, and I. Giaever, “Impedance Analysis of MDCK Cells Measured by Electric Cell-Substrate Impedance Sensing”, *Biophysical journal*, vol. 69, pp. 2800-2807, Dec. 1996.

[15] F. Yu, R. Li, L. Ai, C. Edington, H. Yu, M. Barr, E. S. Kim, T. k. Hsiai, “Electrochemical impedance spectroscopy to assess vascular oxidative stress”, *Annals of Biomedical Engineering*, vol. 39, pp. 287-96, July 2011 [Online] Available: doi: 10.1007/s10439-010-0127-y.

[16] F. Clemente, M. Romano, P. Bifulco, M. Cesarelli, “EIS measurements for characterization of muscular tissue by means of equivalent electrical parameters”, *Measurement*, vol. 58, pp. 476-482, Dec 2014 [Online] Available: doi: 10.1016/j.measurement.2014.09.013.

[17] M. Ducote, B. T. Vinson, S. Hogquist, B. Riggs, J. Saksena and D. B. Chrisey,

“Electrochemical Impedance Spectroscopy (EIS) as a Tool for Pathogen Detection”, *Biotecnologia Aplicada*, Jan. 2009.

[18] C. Skourou , A. Rohr, P. J. Hoopes, K. D. Paulsen, “In vivo EIS characterization of tumor tissue properties is dominated by excess extracellular fluid”, Physics in medicine

and biology, pp. 347-363, Jan. 2007 [Online] Available: doi: 10.1088/0031-9155/52/2/003.

[19] S. Mazlan, M. M. Ramli, M. M. A. B. Abdullah, D. S. C. Halin, S. S. M. Isa, L. F. A. Talip, N. S. Danial, and S. A. Z. Murad, "Interdigitated electrodes as impedance and capacitance biosensors: A review", *AIP Conference Proceedings*, Sept. 2017.

[20] "Applied BioPhysics | Quantifying Cell Behavior," *Applied BioPhysics*. [Online]. Available: http://biophysics.com/about.php. [Accessed: 28-Mar-2019].

[21] A. Rivadeneyra, J. F. Salmerón, A. J. Palma, J. A. López-Villanueva, M. Agudo-Acemel, L. F. Capitan-Vallvey, "Comparative study of printed capacitive sensors", *10th Spanish Conference on Electron Devices (CDE),* 2015.

[22] R. de la Rica, A. Baldi, C. Fernández-Sánchez and H. Matsui, "Selective Detection of Live Pathogens via Surface-Confined Electric Field Perturbation on Interdigitated Silicon Transducers", *Analytical Chemistry,* April 2019. [Online] Available: doi: 10.1021/ac9001854.

[23] *Manual 1260 Impedance/Gain-Phase Analyzer,* Solartron Analytical.

[24] R.Ehret, W.Baumann, M.Brischwein, A.Schwinde and K.Stegbaue, "Monitoring of cellular behaviour by impedance measurements on interdigitated electrode structures", *Biosensors and Bioelectronics,* vol. 12, pp.29-41. 1997.

[25] S. Kima, G. Yub, T. Kima, K. Shinb, J. Yoona, "Rapid bacterial detection with an interdigitated array electrode by electrochemical impedance spectroscopy", *Electrochimica Acta,* vol. 82, pp.126-131, Nov. 2012.

[26] Application note: Basics of electrochemical impedance spectroscopy, Camry Instruments.

[27] J.B, Jorcin, M. E. Orazem, N. Pébère and B. Tribollet, "CPE analysis by local electrochemical impedance spectroscopy", *Electrochimica Acta*, vol. 52, pp. 1473-1479, Jan. 2006.

[28] J.-P. Diard, B. Le Gorrec, C. Montella, *Handbook Of Electrochemical Impedance Spectroscopy ELECTRICAL CIRCUITS CONTAINING CPEs*, [Online]. Available: www.bio-logic.info. [Accessed: 28-Mar-2019].

[29] Equivalent Circuit Models, Camry instruments.

[30] A.V. Mamishev, K. Sundara-Rajan, F. Yang, Y.Q. Du, M. Zahn, “Interdigital sensors and transducers”, *IEEE*, vol. 92, pp. 808–845, 2004. [Online] Avaiable: doi: 10.1109/JPROC.2004.826603.

[31] R. H. Masud Bhuiyan, R. A. Dougal, M. Ali, “Proximity Coupled Interdigitated Sensors to Detect Insulation Damage in Power System Cables”, *IEEE Sensors Journal*, 2007 [Online] Available: doi: 10.1109/JSEN.2007.908440.

[32] T. L Riss, R. A Moravec, A. L Niles, S. Duellman, H. A Benink, T. J Worzella, and L. Minor, “Cell Viability Assays”, *Assay Guidance Manual [Internet],* [Online]. Available: https://www.ncbi.nlm.nih.gov/books/NBK144065/. [Accessed: 20-Mar-2019].

[33] *Manual Alamar Blue Assay*, Invitrogen.

[34] M. Gönczi, N. Szentandrássy, L. Fülöp, A. Telek, G. P. Szigeti, J. Magyar, T. Bíró, P. P. Nánási, L. Csernoch, “Hypotonic stress influence the membrane potential and alter the proliferation of keratinocytes in vitro”, *Experimental dermatology*, Feb. 2017 [Online] Available: doi: 10.1111/j.1600-0625.2006.00533.x

[35] ZView® For Windows [Online]. Avaiable: http://www.scribner.com/software/68-general-electrochemistr376-zview-for-windows/. [Accessed: 10-June-2019].

[36] D. Dam Le, T. N. Nhien Nguyen, D. C. Tin Doan, T. M. Dung Dang and M. Chien Dang, “Fabrication of interdigitated electrodes by inkjet printing technology for application in ammonia sensing”, *Advances in Natural Sciences: Nanoscience and Nanotechnology,* March 2016 [Online] Available: doi: 10.1088/2043-6262/7/2/025002.

[37] M. Singh, H. M. Haverinen, P. Dhagat and G. E. Jabbour, “Inkjet Printing—Process and Its Applications”, *Advanced materials*, Feb. 2010. [Online] Available: doi: 10.1002/adma.200901141.

[38] B. Sadri, D. Goswami and R.V. Martinez, “Rapid Fabrication of Epidermal Paper-Based Electronic Devices Using Razor Printing”, *Micromachines*, vol.9, Aug. 2018. [Online] Avaiable: doi: 10.3390/mi9090420.

[39] T. Miyamoto, S. Takahashi, H. Ito, H. Inagaki and Y. Noishiki, “Tissue biocompatibility of cellulose and its derivatives”, *Journal of biomedical materials research*, vol. 1, pp. 125-133, Jan. 1989. [Online] Avaiable: doi: 10.1002/jbm.820230110.

9. Annexed

9.1 Budget

Table 11. Budget of the project: **consumables**

Material	Cost
Biological consumables **(culture plates, gloves, lab coats, pipettes, pipettes tips, HaCaTs cells, culture media, use of the SEM, gold sputtering…)**	860 € Average cost consulted with the technicians for using the laboratory facilities 5 months
Electronical consumables **(copper tape, cables, Epoxy, Kapton tape (passivator),…)**	49,37 €
Sensors	In collaboration with the Fraunhofer Institute (Germany)

Table 12. Budget of the project: **equipment**

Equipment	Cost
Impedance gain-phase analyzer **(SI 1260)**	7992 € Expected duration: 5 years Cost per month: 133,2 €/month **User cost (3 months): 399,6 €**
Impedance gain-phase analyzer **(ISX-3mini)**	8600 € Expected duration: 5 years Cost per month: 143,33 €/month **User cost (2 months): 286,67 €**
Picoamperimeter **(KEITHLEY 6487)**	4076,17€ € Expected duration: 5 years Cost per month: 67,94 €/month

	User cost (1 month): 67,94 €

Table 13. Budget of the project: **licenses**

License	Cost & Cost per user
Zview licence	Total cost of the undefined license: 1421,05 € Expected duration of the license: 3 years Cost per month: 39,47 €/month **User cost (4 months): 157,89 €**
Zplot licence	Total cost of the undefined license: 2210,00€ Expected duration of the license: 3 years Cost per month: 61,39 €/month **User cost (5 months): 306,94 €**
OriginPro licence	1-year student license: 61,24 €
Microsoft Word, Excel and PowerPoint licenses (pack)	1-year student license: 106,40€
SPSS Statistics license	88,26€/month, per user: **User cost (2 months): 176,52 €**

Table 14. Budget of the project: **man power**

Personnel	Cost
Rosario Quevedo de Cea **(undergraduate student)**	Total number of hours employed: 1 year, 80 hours/month Salary per month: none
Cristina Moral Gil **SEM technician**	Total number of hours employed: 5h in total. Salary: 15€/hour 75 €

Total cost of the Bachelor Thesis:	2547,57 €

9.2 Project scheduling

The following Gantt diagram was created with the Free Edition of teamgantt webpage[1].

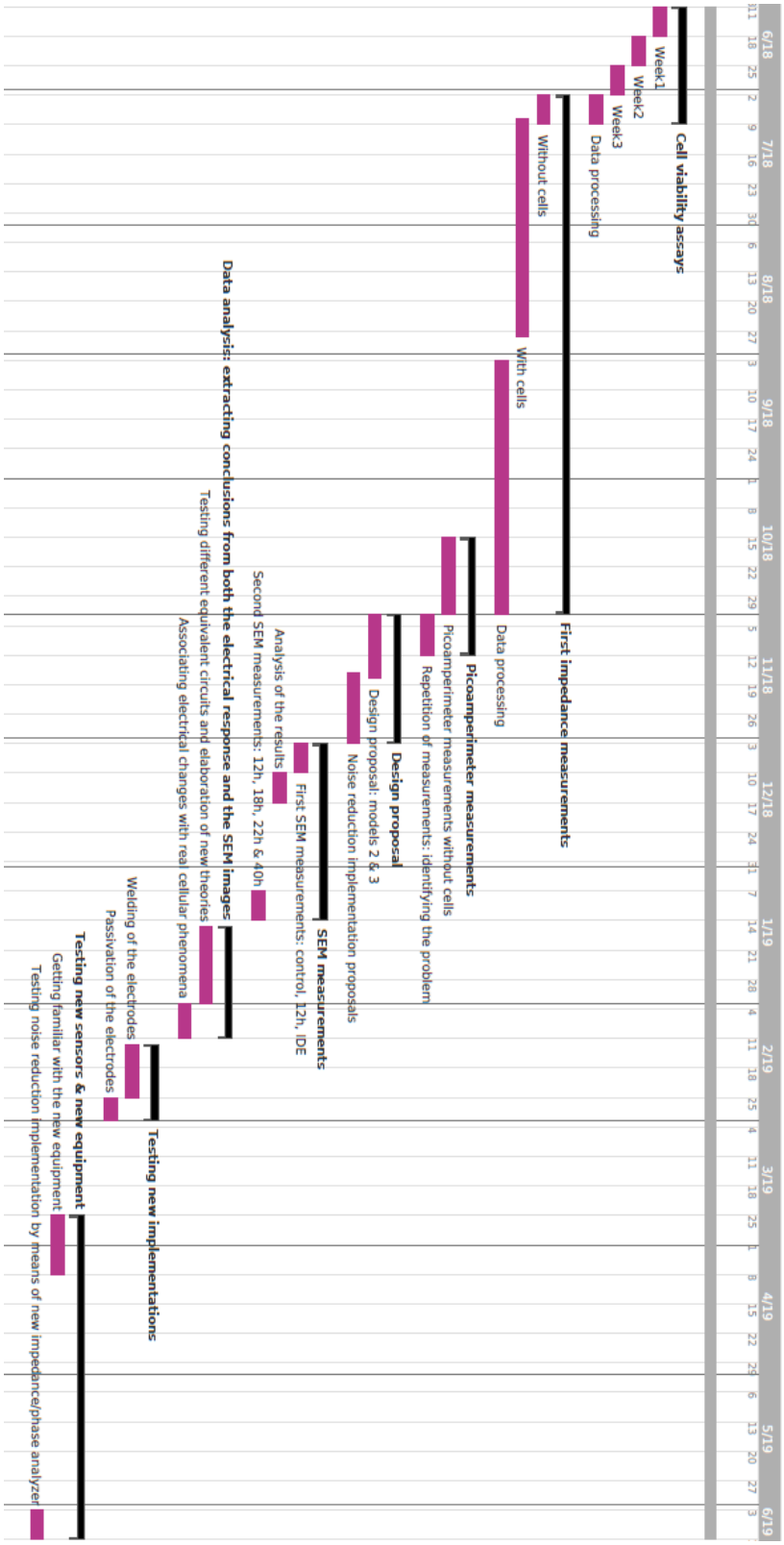

Figure 48. Gantt diagram representing the schedule of this Bachelor Thesis.

[1] https://www.teamgantt.com/